Critical Casimir effect in superfluid wetting films

A. Maciołek,[1,2,3] A. Gambassi,[1,2] and S. Dietrich[1,2]

[1]*Max-Planck-Institut für Metallforschung, Heisenbergstrasse 3, D-70569 Stuttgart, Germany*
[2]*Institut für Theoretische und Angewandte Physik, Universität Stuttgart, Pfaffenwaldring 57, D-70569 Stuttgart, Germany*
[3]*Institute of Physical Chemistry, Polish Academy of Sciences, Kasprzaka 44/52, PL-01-224 Warsaw, Poland*

Recent experimental data for the complete wetting behavior of pure ^{4}He and of ^{3}He-^{4}He mixtures exposed to solid substrates show that there is a change of the corresponding film thicknesses L upon approaching thermodynamically the λ transition and the tricritical end point, respectively, which can be attributed to critical Casimir forces f_C. We calculate the scaling functions ϑ of f_C within models representing the corresponding universality classes. For the mixtures our analysis provides an understanding of the rich behavior of ϑ deduced from the experimental data and predicts the crossover behavior between the tricritical point and the λ transition of pure ^{4}He which are connected by a line of critical points. The formation of a "soft-mode" phase within the wetting films gives rise to a pronounced maximum of f_C below the tricritical point as observed experimentally. Near the tricritical point we find logarithmic corrections $\sim L^{-3}(\ln L)^{1/2}$ for the leading behavior of ϑ dominating the contributions from the background dispersion forces.

I. INTRODUCTION

There is growing experimental evidence for the analog of the electromagnetic Casimir effect [1] in various critical condensed matter systems [2–7]. In wetting experiments the confinement of critical fluctuations within an adsorbed liquid film gives rise to an effective Casimir force f_C between the substrate-liquid and the liquid-vapor interfaces of the liquid film [8–10]. Near the critical end point of the liquid the emerging Casimir force adds to the omnipresent dispersion forces and thus leads to a change of the thickness of the complete wetting film. From this response one can infer the Casimir force by subtracting the effect of the background forces which varies smoothly near the critical end point with temperature T_c. In accordance with finite-size scaling theory [11] this force f_C per unit area and in units of $k_B T_c$ can be expressed in terms of a universal scaling function ϑ; its shape depends sensitively on the type of boundary conditions (BCs) [9] and thus on the surface universality classes the confining surfaces belong to [12].

Capacitance measurements of the equilibrium thickness of ^{4}He wetting films near the superfluid temperature T_λ of the critical end point of the λ line [2,7] quantitatively support the theoretical predictions of f_C for the bulk universality class of the *XY* model with *symmetric* Dirichlet-Dirichlet BCs (O, O) forming the so-called ordinary (O) surface universality class [12]. Such BCs correspond to the case that the quantum-mechanical wave function of the superfluid state vanishes at both interfaces, giving rise to an attractive Casimir force ($f_C < 0$) [9,10]. However, the available theoretical results have a limited range of applicability, i.e., $T \gtrsim T_\lambda$ and $T \ll T_\lambda$. Above and at T_λ explicit field-theoretical calculations within the ϵ-expansion scheme are available [13,14]. For temperatures well below T_λ there are calculations which take into account capillary-wavelike surface fluctuations in the asymptotic limit of thick films, predicting a leveling off of the scaling function for large negative scaling variables [15], i.e., $T \ll T_\lambda$, in qualitative agreement with the experimental

observations. So far there are no theoretical results available for the critical region below T_λ which provide an understanding of the deep minimum of the experimental scaling function (approximately 20 times deeper than its value at T_λ).

^{3}He-^{4}He mixtures near their tricritical end point (see Fig. 12 in Ref. [14]) are another critical system for which wetting experiments have been performed recently [4,5]. The tricritical end point with temperature T_t is the point in the ^{3}He-^{4}He phase diagram where the line signalling the onset of superfluidity joins the top of the two-phase coexistence region for phase separation into a ^{4}He-rich superfluid phase and a ^{3}He-rich normal phase. The mixture belongs to a bulk universality class different from that of pure ^{4}He and, because its upper critical spatial dimension d^* equals 3, the actual physical system is characterized by rational mean-field critical exponents (up to logarithmic corrections) [16,17]. The capacitance measurements of the wetting film thickness of the mixture reveal a *repulsive* Casimir force f_C around the tricritical end point which suggests *nonsymmetric* BCs for the superfluid order parameter (OP). The probable physical mechanism behind such a BC is that within ^{3}He-^{4}He wetting films a ^{4}He-rich layer forms near the substrate-liquid interface, which may become superfluid already above the line of onset of superfluidity in the bulk [18] whereas the lighter ^{3}He has a preference for the liquid-vapor interface. Thus the two interfaces impose a nontrivial concentration profile which in turn couples to the superfluid OP.

For this system, recently [19] we briefly reported explicit model calculations which demonstrate that the concentration profile indeed induces indirectly *nonsymmetric* BCs for the superfluid OP. For symmetry-breaking (+) BCs at the substrate-liquid interface and Dirichlet (O) BCs at the liquid-vapor interface we calculated the Casimir force and found a semiquantitative agreement with the experimental data given in Ref. [4]. Moreover, we formulated theoretical predictions for the behavior of f_C in the crossover regime between the tricritical point and the λ transition of pure ^{4}He which are connected by a line of critical points and provided the uni-

versal leading behavior of the Casimir force at the tricritical point.

The purpose of the present study is to elucidate the details of the two complementary approaches used in Ref. [19] and to extend them in order to obtain additional results both for the tricritical ^{3}He-^{4}He mixture and the critical pure ^{4}He. The presentation is organized as follows: In Sec. II we discuss the universal properties of the Casimir force. As already mentioned above, for the present tricritical behavior the upper critical dimension d^* equals 3 and therefore the thermodynamic functions of three-dimensional systems exhibit power-law behaviors with critical exponents taking their classical values. However, logarithmic corrections to the mean-field (MF) behavior are expected under experimental conditions [17]. Using field-theoretical methods and renormalization-group (RG) analyses we obtain the leading asymptotic behavior of the Casimir force at the tricritical point. As a function of the film thickness L it has the form of a power law multiplied by a fractional power of a logarithm and by the *universal* Casimir amplitude. In addition, we also derive the form of the finite-size scaling for the Casimir force in the vicinity of the tricritical point. As expected [17], also the arguments of the associate scaling function acquire logarithmic corrections. These scaling functions are compared with the ones deduced from the experimental data in Ref. [4]. In Sec. III we study within mean-field theory (MFT) films of the lattice vectoralized Blume-Emery-Griffiths (VBEG) model [20] which belongs to the same universality class as the ^{3}He-^{4}He mixture but is simple enough to allow for systematic studies of f_C along all thermodynamic paths followed in the wetting experiments of Ref. [4]. This facilitates the exploration of the crossover between the tricritical point T_t and the line of critical points and the coexistence region below T_t. This enables us to follow the Casimir force upon continuously switching the bulk universality class (from tricritical to critical) by changing the concentration of the ^{3}He-^{4}He mixture. The scaling functions corresponding to thermodynamic paths of constant concentration of the two components of the ^{3}He-^{4}He mixtures are calculated and compared with the corresponding experimental data in Ref. [4]. As a limiting case the VBEG model can describe also a film of pure ^{4}He which is studied in Sec. IV within MFT. The scaling function of the corresponding Casimir force is obtained in the critical region below T_λ and compared with that extracted from the experimental data in Ref. [2]. We also compare these results with the mean-field predictions which follow from the Landau-Ginzburg theory in the film geometry with suitable BCs. In Sec. V we discuss the theoretical results obtained within the VBEG model and assess their relevance for interpreting the experimental data. We conclude with a summary and an outlook in Sec. VI.

II. UNIVERSAL PROPERTIES

For film geometries, in this section we investigate the universal properties of the Casimir force near tricriticality. In general two-component systems are characterized by the ordering density $\mathbf{\Phi}$ and its conjugate field h, and by a nonordering density x and its conjugate field Δ. For liquid ^{3}He-^{4}He

mixtures, $\mathbf{\Phi}$, x, and Δ correspond to the superfluid OP, to the ^{3}He concentration, and to the difference between the chemical potentials of the ^{3}He and ^{4}He components, respectively, whereas the field h conjugate to the superfluid OP is experimentally not accessible.

A. Scaling function from Landau-Ginzburg theory

In order to capture universal properties we consider the standard dimensionless $O(n)$-symmetric Landau-Ginzburg (LG) Hamiltonian for a tricritical system in the film geometry:

$$\mathcal{H}[\mathbf{\Phi}] = \int d^{d-1}x \int_0^L dz \left\{ \frac{1}{2}(\nabla\mathbf{\Phi})^2 + \frac{r_0}{2}\mathbf{\Phi}^2 \right.$$
$$\left. + \frac{u_0}{4!}(\mathbf{\Phi}^2)^2 + \frac{v_0}{6!}(\mathbf{\Phi}^2)^3 \right\}, \qquad (1)$$

where L is the film thickness, $\mathbf{\Phi}$ is the n-component order parameter (OP) ($n=2$ corresponds to the XY universality class), and z is the coordinate normal to the confining surfaces; r_0, u_0, and v_0 are bare coupling constants depending, *inter alia*, on the temperature T and the nonordering field Δ. $r_0(u_0)=0$ and $u_0>0$ define the critical line, whereas at the tricritical point one has $r_0=u_0=0$, $v_0>0$. The semi-infinite version of Eq. (1) has been studied in the context of surface critical behavior [21]. In the film geometry the Casimir force per area A of the cross section of the film and in units of $k_B T_t$,

$$f_C \equiv -(\partial f^{ex}/\partial L) = \langle \mathcal{T}_{zz} \rangle, \qquad (2)$$

is given by the thermal average of the stress tensor component $\mathcal{T}_{zz}$ [9]:

$$f^{ex}(L) \equiv (f - f_b)L/(k_B T_t), \qquad (3)$$

where f is the total free energy of the film per volume $V = LA$ and f_b is the bulk free energy density. For large L the excess free energy can be decomposed into surface and finite-size contributions: $f^{ex}(L) = f_{s,1} + f_{s,2} + \delta f(L)$. The stress tensor is given by [9]

$$\mathcal{T}_{ij} = \partial_i \mathbf{\Phi} \cdot \partial_j \mathbf{\Phi} - \delta_{ij}\mathcal{L} - (d-2)/[4(d-1)](\partial_i\partial_j - \delta_{ij}\nabla^2)\mathbf{\Phi}^2, \qquad (4)$$

where $\mathcal{L}$ is the integrand in Eq. (1). In what follows we assume $\mathbf{\Phi} = (m(z), 0, \ldots, 0)$, i.e., we neglect helicity. For nonsymmetric BC its relevance for the behavior of the Casimir force is not clear because the OP has the additional freedom to rotate across the film by a position dependent angle $\phi(z)$; the analyses of the role of helicity is left for future research. Within MFT for the LG Hamiltonian, the determination of the tricritical Casimir force in the film geometry starts from the Euler-Lagrange equation

$$m''(z) = r_0 m(z) + \frac{u_0}{6}m^3(z) + \frac{v_0}{120}m^5(z). \qquad (5)$$

As discussed in Sec. I, $(+, O)$ boundary conditions, with the substrate at $z<0$ and vapor at $z>L$,

$$m(0) = +\infty \quad \text{and} \quad m(L) = 0 \tag{6}$$

are supposed to mimic the experimental system of ^{3}He-^{4}He wetting films as studied in Ref. [4]. According to Eq. (4) the stress tensor component $\mathcal{T}_{zz}$ evaluated within MFT and with $\Phi = (m(z), 0, \ldots, 0)$ for the OP (in the present MF approach we omit the brackets $\langle \cdot \rangle$ indicating the thermal average) yields

$$\mathcal{T}_{zz} = \frac{1}{2}[m'(L)]^2. \tag{7}$$

In deriving this expression we have used the property that $\mathcal{T}_{zz} = \text{const}$ throughout the film including the surfaces and we have chosen $z_0 = L$ as the point of reference at which $\mathcal{T}_{zz}$ is evaluated. Accordingly, the first integral of Eq. (5) is given by

$$[m'_{+,O}(z)]^2 = 2\mathcal{T}_{zz} + r_0 m^2_{+,O}(z) + \frac{u_0}{12}m^4_{+,O}(z) + \frac{v_0}{360}m^6_{+,O}(z). \tag{8}$$

Dimensional analysis yields that, at the upper critical dimension $d = d^* = 3$, $m(z, L, r_0, u_0, v_0)$ can be expressed in terms of a dimensionless scaling function $\varphi_{+,O}$:

$$m_{+,O}(z, L, r_0, u_0, v_0) = \left(\frac{v_0}{360}\right)^{-1/4} L^{-1/2} \varphi_{+,O}(z/L, r_0L^2, u_0L; v_0), \tag{9}$$

where v_0 is dimensionless. Similarly, within this approach the normalized Casimir force can be expressed in terms of a dimensionless scaling function $\vartheta^{MF}_{+,O}$:

$$\mathcal{T}_{zz} = f_C(L, r_0, u_0, v_0) = \left(\frac{v_0}{90}\right)^{-1/2} L^{-3} \vartheta^{MF}_{+,O}(r_0L^2, u_0L, v_0). \tag{10}$$

Equation (8) can be written in terms of these scaling functions $\varphi_{+,O}$ and $\vartheta^{MF}_{+,O}$:

$$[\varphi'_{+,O}(x)]^2 = \vartheta^{MF}_{+,O} + r_0L^2\varphi^2_{+,O}(x) + \left(\frac{5}{2v_0}\right)^{1/2} u_0L\varphi^4_{+,O}(x)$$
$$+ \varphi^6_{+,O}(x), \tag{11}$$

where $x = z/L$. In turn, Eq. (11) can be integrated directly yielding the implicit equation

$$1 = \int_0^\infty \frac{d\varphi}{\sqrt{\vartheta^{MF}_{+,O} + r_0L^2\varphi^2 + \left(\frac{5}{2v_0}\right)^{1/2} u_0L\varphi^4 + \varphi^6}} \tag{12}$$

for the scaling function $\vartheta^{MF}_{+,O}(r_0L^2, u_0L, v_0)$. Note that the coupling constant $v_0 > 0$ remains undetermined within mean-field theory and enters into $\vartheta^{MF}_{+,O}$ only in the combination $v_0^{-1/2}u_0L$. Under the renormalization group flow, at the upper critical dimension $(d^* = 3)$ the renormalized coupling constant v associated with v_0 tends to its fixed point value v^* $= 0$. This RG flow generates logarithmic corrections to scaling due to the singular dependence of the scaled quantities on v [see, e.g., Eqs. (9) and (10)]. With the transformation

$$\varphi = (\vartheta^{MF}_{+,O})^{1/6}p \tag{13}$$

for the integration variable one can rewrite Eq. (12) in the more convenient but still implicit form

$$(\vartheta^{MF}_{+,O})^{1/3} = \int_0^\infty \frac{dp}{\sqrt{1 + ap^2 + bp^4 + p^6}}, \tag{14}$$

where the dimensionless parameters a and b are given by

$$a = r_0L^2(\vartheta^{MF}_{+,O})^{-2/3} \quad \text{and} \quad b = \left(\frac{5}{2v_0}\right)^{1/2} u_0L(\vartheta^{MF}_{+,O})^{-1/3}. \tag{15}$$

The numerical evaluation of the scaling function amounts to the following steps: (i) specifying values for a and b, (ii) evaluating $\vartheta^{MF}_{+,O}$ from Eq. (14), (iii) determining the values of the two scaling variables r_0L^2 and $v_0^{-1/2}u_0L$ from Eq. (15).

From the symmetry properties of the order-parameter profile for the symmetry breaking opposing boundary conditions $(+,-)$ it is obvious that within MFT the force for a film of thickness L in this case can be obtained from Eq. (14), holding for the $(+,O)$ BC, and Eq. (10) by replacing $L \mapsto L/2$ therein. This implies $\vartheta^{MF}_{+,-}(x, y) = 8\vartheta^{MF}_{+,O}(x/4, y/2)$. In the following we shall refer only to the $(+,O)$ BC and drop the corresponding index.

The precise dependence of r_0 and u_0 on the thermodynamic fields T and Δ is not known. Therefore it is not obvious how to follow in terms of these variables a specified path in the phase diagram such as the experimental path of fixed ^{3}He concentration. However, assuming that r_0 and u_0 are analytic functions of T and Δ in the neighborhood of the phase transition one can use the expansion [17]:

$$r_0 = A(\Delta)[T - T_\lambda(\Delta)] + O([T - T_\lambda(\Delta)]^2) \quad \text{and}$$

$$u_0 = B(\Delta) + O([T - T_\lambda(\Delta)]), \tag{16}$$

where $T_\lambda(\Delta)$ denotes the critical temperatures of the line of continuous phase transitions as a function of Δ, and $B(\Delta)$ and $A(\Delta)$ are positive and nonzero on this line; $B(\Delta) = 0$ at the tricritical point.

In view of comparisons with experimental data, which we shall discuss later, it is useful to mention the relation between the parameters r_0 and u_0 and the experimentally controllable thermodynamic fields $T - T_t$ and $\Delta - \Delta_t$ where $\Delta = \Delta_t$ at the tricritical point and $T_\lambda(\Delta_t) = T_t$. These "deviating fields" are not the proper scaling fields and it was shown [22] that a suitable (dimensionless) choice is provided by

$$t \equiv (T - T_t)/T_t \quad \text{and} \quad g \equiv (\Delta - \Delta_t)/(k_BT_t) + a't, \tag{17}$$

where a' is the slope of the line tangential to the phase boundary at the tricritical point. Thus for $t \to 0$ with $g = 0$ the tricritical point is approached tangentially to the phase boundary. Instead of t one could also use a scaling variable which is orthogonal to the loci $g = 0$; this would not affect the leading singular behavior for $t, g \to 0$ [17]. Near the tricritical point $B(\Delta)$, $A(\Delta)$, and $T_\lambda(\Delta)$ can be expanded in terms of g

and t. Using Eq. (17) one has $T-T_\lambda(\Delta)=T-T_t+(a'k_B)^{-1}(\Delta-\Delta_t)+O((\Delta-\Delta_t)^2)=(a')^{-1}T_t g+O((\Delta-\Delta_t)^2)$. Expressing Δ and T as a function of t and g one finds

$$r_0 = A_1 g + A_2 t^2 + O(g^2, gt) \quad \text{and}$$

$$u_0 = B_1 t + B_2 g + O(gt, g^2, t^2), \tag{18}$$

where $A_1 > 0$, $B_1 > 0$, A_2, and B_2 are constants. Due to the analytic structure of Eq. (16) and because $(\Delta-\Delta_t)=k_B T_t(g-a't)$ the coefficient r_0 does not contain a term linear in t so that $u_0 \sim t + O(t^2)$ if $r_0 = 0$. On the other hand, $r_0 \sim g + O(g^2)$ if $u_0 = 0$.

B. Logarithmic corrections at $T = T_t$

At the tricritical point $a = b = 0$ Eq. (14) reduces to

$$(\vartheta^{MF})^{1/3} = \int_0^\infty dp/\sqrt{1+p^6} \simeq 1.402\,18. \tag{19}$$

Accordingly, in units of $Ak_B T_t$, the MFT result for the tricritical Casimir force f_C^t in the case of the $(+,O)$ BC is [see Eq. (10)]

$$f_{C,t}^{MF} \simeq 2.756\,84(90/v_0)^{1/2}L^{-3}. \tag{20}$$

In $d = 3 - \epsilon$ the MFT result at tricriticality [Eq. (20)] yields the leading contribution in a perturbation series, i.e.,

$$\langle \mathcal{T}_{zz} \rangle = \langle \mathcal{T}_{zz} \rangle_0 + \langle \mathcal{T}_{zz} \rangle_1 + O(v_0^{1/2})$$

$$= \left(\frac{v_0}{90}\right)^{-1/2} t_{zz} + \langle \mathcal{T}_{zz} \rangle_1 + O(v_0^{1/2}), \tag{21}$$

where both $t_{zz} \equiv 2.756\,84 L^{-3}$ and $\langle \mathcal{T}_{zz} \rangle_1$ do not depend on v_0. After removing ultraviolet singularities via renormalization (R) the asymptotic scaling behavior of f_C follows from substituting the renormalized v by the appropriate fixed-point value $v^* \propto \epsilon$. At $d = d^*$, and under spatial rescaling by a dimensionless factor ℓ, v flows to its RG fixed point value $v^* = 0$ according to [21]

$$\bar{v}(\ell) = \frac{240\pi^2}{3n+22}\left(\frac{1}{|\ln \ell|} + c\,\frac{\ln|\ln \ell|}{\ln^2 \ell} + \cdots\right), \tag{22}$$

where $\bar{v}(\ell)$ is the running coupling constant with the initial condition $\bar{v}_R(\ell = 1) = v_R$. With the rescaling factor $\ell = l_0/L$, where l_0 is a microscopic length scale of the order of a few Å, this yields a logarithmic correction to the power-law dependence on L of the tricritical Casimir force:

$$f_C^t \simeq 0.54(3n+22)^{1/2}[\ln(L/l_0)]^{1/2}L^{-3}$$

$$\times \left(1 - \frac{c}{2}\frac{\ln|\ln(L/l_0)|}{|\ln(L/l_0)|} + \cdots\right). \tag{23}$$

Determining the constant c requires to extend the analysis in Ref. [21] which is left for future research. Gaussian fluctuations give contributions of at least $O(v^0)$ which are therefore of order L^{-3} and thus subdominant [see Eq. (23)]. We compare Eq. (23) for $n = 2$ with the data obtained by Garcia and Chan [4] for their experimental value of $L \approx 520$ Å and for

$l_0 \approx 1.3$ Å, the experimental value of the correlation length amplitude $\zeta_0 = \zeta(t)/|t|^{-\nu_t}$ with $\nu_t = 1$ for *concentration* fluctuations below T_t in the superfluid phase [23]. For these values Eq. (23) predicts

$$\vartheta_t \equiv f_C^t L^3 \approx 6.96 \tag{24}$$

whereas $\vartheta_t^{exp} = 8.4 \pm 1.7$. The value of the theoretical function ϑ_t at T_t, with l_0 between 1 and 2 Å, is in reasonable agreement with the measured ϑ_t^{exp}. In order to extract the actual value of the *universal* Casimir amplitude [i.e., the numerical prefactor $0.54\sqrt{28} = 2.86$ in Eq. (23)] the experimental data call for a re-analysis based on the functional form given by Eq. (23), which renders the comparison independent of the choice for l_0, and requires us to take into account the correction terms given in Eq. (23). We want to emphasize that the tricritical Casimir force offers the opportunity to observe the so far experimentally elusive logarithmic corrections associated with tricritical phenomena. We note that *at tricriticality* the Casimir force $f_C^t(L \to \infty)$ dominates over the background dispersion forces. This differs from the case of *critical* Casimir forces for which both contributions decay with the same power law. It is interesting that the Casimir amplitude for the present $(+,O)$ BC is the same as for the $(+,+)$ BC considered in Ref. [24].

C. Logarithmic corrections to the scaling function

The scaling properties of the Casimir force follow from the renormalized finite-size contribution to the excess free energy [Eq. (3)]. For carrying out the renormalization procedure of this quantity two aspects are relevant. First, for the film geometry, the width L of the system is not renormalized [11]. Second, in the renormalized (R) finite-size contribution to the free energy $\delta f(L)$ [see the text before Eq. (4)] the contributions from the additive counter terms cancel and one has [12,25]:

$$\delta f^R(r,u,v;\mu,L) = \delta f(r_0,u_0,v_0;L), \tag{25}$$

where the bare quantities u_0, r_0, and v_0 are expressed in terms of renormalized ones r, u, and v; μ is an arbitrary momentum scale. Since we are not considering correlation functions at the surface, all renormalization factors Z are the same as those in the bulk [12,21]:

$$r_0 = Z_r r + u^2 \mu^{-2\epsilon}P, \quad u_0 = Z_u u, \quad v_0 = 2\pi^2 Z_v v, \tag{26}$$

where the dimensions of the coupling constant are $[r_0] = \mu^2$, $[u_0] = \mu^{1+\epsilon}$, and $[v_0] = \mu^{2\epsilon}$. Explicit perturbative results for the tricritical bulk renormalization functions Z_r, P, Z_u, and Z_v are known (see, e.g., Refs. [17,21]). From Eq. (25) the RG equation can be derived in a standard fashion by exploiting the fact that $\delta f(r_0,u_0,v_0;L)$ is independent of μ. Because in Eq. (25) there are no additive renormalization terms it follows that $\delta f^R(L)$ satisfies the following homogeneous RG equation [12]:

$$\left[\mu\,\partial_\mu + \sum_{\kappa=r,u,v} \beta_\kappa \partial_\kappa\right]\delta f^R(L) = 0, \tag{27}$$

where $\beta_\kappa(r,u,v;\epsilon) \equiv \mu\partial_\mu|_0 \kappa$ and $\partial_\mu|_0$ denotes derivatives with respect to μ at fixed bare interaction constants for κ

$=r,u,v$. The RG equation is solved by using the method of characteristics (see, e.g., Ref. [26]):

$$\delta f^R(r',u,v,\mu;L) = \delta f^R(\bar{r}'(\ell),\bar{u}(\ell),\bar{v}(\ell);\mu\ell,L), \quad (28)$$

where ℓ is again a dimensionless spatial rescaling factor, $\bar{\kappa}(\ell)$ are the running coupling constants with the initial condition $\bar{\kappa}(1)=\kappa$, and due to the form of the renormalization of r_0 [see Eq. (26)] the new variable r' is given by [17,21]

$$r' = r + w(v,\mu)u^2. \quad (29)$$

For an explicit expression of $w(v,\mu)$ see Refs. [17,21]. Equation (28) summarizes the RG transformation and the nonrenormalization of L. Using dimensional analysis one obtains

$$\delta f^R(r',u,v,\mu;L)$$
$$= (\mu\ell)^{(d-1)}\delta f^R\left(\frac{\bar{r}'(\ell)}{(\mu\ell)^2},\frac{\bar{u}(\ell)}{(\mu\ell)^{4-d}},\frac{\bar{v}(\ell)}{(\mu\ell)^{2(3-d)}};1,L\mu\ell\right).$$
$$(30)$$

The desired asymptotic scaling behavior of δf^R follows by substituting on the right-hand side of Eq. (30) the appropriate fixed-point values for the running coupling constants $\bar{r}'$, $\bar{u}$, and $\bar{v}$. The infrared stable fixed point lies at $v^*=[240/(3n+22)]\epsilon+O(\epsilon^2)$ [21]. Upon approaching the upper critical dimension $v^*\to0$ and for $\epsilon\to0$ the relevant logarithmic corrections to the classical exponents are generated by the flow of the coupling constants under the RG transformation $\ell\to0$. In the limit $\ell\to0$, $\bar{v}(\ell)$ is given by Eq. (22). The running variables $\bar{r}'(l)$ and $\bar{u}(l)$ can be written as $\bar{r}'(\ell)=E_r(\ell;v)r'$ and $\bar{u}(\ell)=E_u(\ell;v)u$. A straightforward analysis [17,21] shows that $E_r(\ell;v)\to$const and $E_u(\ell;v)\sim|\ln\ell|^{-2(n+4)/(3n+22)}$ for $\ell\to0$. Choosing $\mu=1/l_0$, $\mu\ell L=\ell(L/l_0)=1$, and omitting the constant factor E_r we obtain the following scaling form for δf:

$$\delta f^R(r',u,v,\mu;L)$$
$$= L^{-2}\delta f^R(r'L^2,uL|\ln(L/l_0)|^{-2(n+4)/(3n+22)},|\ln(L/l_0)|^{-1};1,1).$$
$$(31)$$

Due to Eq. (2) the scaling form for the Casimir force follows from Eq. (31) as

$$f_C(r',u,v;L)$$
$$\simeq L^{-3}\theta(r'L^2,uL|\ln(L/l_0)|^{-2(n+4)/(3n+22)},|\ln(L/l_0)|^{-1}).$$
$$(32)$$

The scaling function θ is given in terms of $\delta f^R(z_1,z_2,z_3,1)$ as $\theta=2\delta f^R+2z_1(\partial\delta f^R/\partial z_1)-z_2(\partial\delta f^R/\partial z_2)$. The higher-order terms neglected in Eq. (32) are of the form

$$L^{-3}[\ln(L/l_0)]^{-1}[2(n+4)/(3n+22)]z_2(\partial\delta f^R/\partial z_2)$$
$$+ L^{-3}[\ln(L/l_0)]^{-1}z_3(\partial\delta f^R/\partial z_3)+L^{-3}[-1$$
$$+ 2c(\ln|\ln(L/l_0)|)/\ln^3|(L/l_0)|](\partial\delta f^R/\partial z_3).$$

The third term in the latter expression stems from the correction to z_3 [see Eqs. (30) and (22)].

At the upper critical dimension the asymptotic critical behavior obtained from the perturbative RG calculations within the Gaussian approximation is expected to be exact. However, at the lowest order, often referred to as renormalized mean-field theory (RMF)—which yields the free energy correctly with the leading logarithms—one neglects the contributions stemming from the Gaussian fluctuations and replaces the scaling function by its mean-field-like form but with the rescaled arguments.

Applying this reasoning to the free energy we use the mean-field result given by Eqs. (10) and (12) with r_0 replaced in favor of r' according to Eq. (29) with $w(\bar{v}(\ell),\mu(\ell))\to$const as $\ell\to0$, u_0 replaced by $u|\ln(L/l_0)|^{-2(n+4)/(3n+22)}$, and v_0 replaced by $[(240\pi^2)/(3n+22)]|\ln(L/l_0)|^{-1}$ to obtain at lowest order

$$f_C^{RMF}\simeq\left(\frac{3n+22}{8\pi^2/3}\right)^{1/2}[\ln(L/l_0)]^{1/2}L^{-3}$$
$$\times\vartheta^{MF}(r'L^2,uL|\ln(L/l_0)|^{-2(n+4)/(3n+22)},|\ln(L/l_0)|^{-1}).$$
$$(33)$$

In the following we want to compare the behavior of the MF and RMF expression for the Casimir force. As we have already stressed before, f_C calculated within the MF approach depends on the nonuniversal and dimensionless parameter v_0 [see Eq. (10)]. Upon comparing with experimental data this parameter can be used to fit the amplitude of the Casimir force, because $v_0^{-1/2}$ appears (albeit not exclusively) as a prefactor of the scaling function. The factor $v_0^{-1/2}$, which multiplies the coupling constant u_0 [see the text after Eq. (12)], is absorbed in the definition of the scaling variable.

In Fig. 1 we have plotted two curves: (i) $\bar{\vartheta}^{MF}(r_0L^2=0,y^{MF})=f_CL^3(v_0/90)^{1/2}$ as a function of $y^{MF}=[5/(2v_0)]^{1/2}u_0L$ [see Eq. (12)]. Here, the nonuniversal factor $v_0^{-1/2}$ is absorbed in the definitions of the scaling function and of the scaling variable. As already mentioned before $u_0\sim t$ if $r_0=0$, so that $u_0L\sim tL$. (ii) $f_CL^3\equiv\bar{\vartheta}^{RMF}(0,y^{RMF})=[28/(8\pi^2/3)]^{1/2}[\ln(L/l_0)]^{1/2}\vartheta^{MF}(0,y^{RMF})$ (for $n=2$), where $y^{RMF}=uL[\ln(L/l_0)]^{1/14}$. Here, renormalization fixes the amplitude of the Casimir force replacing the nonuniversal prefactor $\left(\frac{v_0}{90}\right)^{-1/2}$ [see Eq. (10)] of the scaling function by the amplitude and the logarithmic correction to the L dependence. The scaling variable y^{RMF} includes the logarithmic correction $|\ln(L/l_0)|^{-2(n+4)/(3n+22)}$ to u and the additional logarithmic term $|\ln(L/l_0)|^{1/2}$ stemming from the factor $[5/(2v_0)]^{1/2}$ [see y^{MF} and Eq. (12)]. The numerical factor $7/(24\pi^2)$ has been included in the definition of u. For comparison with experimental data this factor can be combined with the nonuniversal constant of proportionality between u and t. For the plot we have chosen the experimental value for L/l_0, i.e., 520 Å/1.3 Å. The shapes of both scaling functions are similar but the RMF result gives the correct value for the Casimir amplitude and the correct L dependence of the scaling function. This should be helpful for interpreting experimental data obtained for different film thicknesses.

In Fig. 2 we show the corresponding results for $u=0$ so that $r'=r$ [see Eq. (29)], $r\sim t$, and $rL^2\sim gL^2$. We find that for
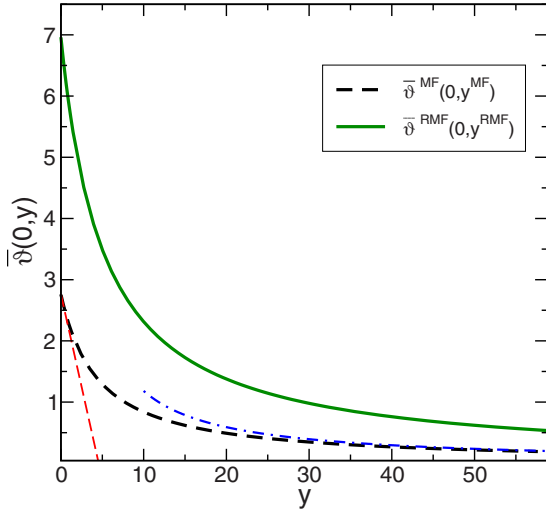
FIG. 1. (Color online) Dimensionless MF scaling function $\bar{\vartheta}^{MF}(r_0 L^2 = 0, y^{MF}) = f_C L^3 (v_0/90)^{1/2}$ [see Eq. (10)] with $y^{MF} = [5/(2v_0)]^{1/2} u_0 L \sim tL$ plotted together with the renormalized mean-field scaling function $f_C L^3 = \bar{\vartheta}^{RMF}(0, y^{RMF})$ [see Eq. (33) and the main text] with $y^{RMF} = \hat{u} L [\ln(L/l_0)]^{1/14}$, $\hat{u} = 7u/(24\pi^2)$, and $L/l_0 = 400$. $\bar{\vartheta}^{MF}(0, y^{MF} \to \infty) \simeq 11.82/y^{MF}$ (thin dash-dotted line) and $\bar{\vartheta}^{MF}(0, y^{MF} \to 0) \simeq 2.76 - 0.605 y^{MF}$ (thin dashed line). The asymptotic behavior of $\bar{\vartheta}^{RMF}(0, y^{RMF})$ can be obtained from the one of $\bar{\vartheta}^{MF}(0, y^{MF})$ by multiplying the ordinate by the factor $[28/(8\pi^2/3)]^{1/2}[\ln(L/l_0)]^{1/2}$ and the abscissa by the factor $[\ln(L/l_0)]^{1/14}$. These limiting behaviors have been inferred from asymptotic expansions of Eq. (14).

$u = 0$ both scaling functions decay much faster to zero than for $r = 0$.

For $r_0 = 0$ one has $u \sim t$ so that, up to the logarithmic corrections, the scaling function $\bar{\vartheta}^{MF}(0, y^{MF})$ should correspond to the experimental curve $\vartheta(tL)$ in Fig. 3 for the tricritical concentration [4]. (We note that the argument of the experimental curve is given in units of Å.) The solid line in this figure represents $\bar{\vartheta}^{MF}(0, y^{MF})$ suitably adjusted with respect to the parameter v_0 such that the Casimir amplitude and the position of the maximum equal the experimental ones [4].

III. VECTORALIZED BLUME-EMERY-GRIFFITHS MODEL

Based on the motivation provided in the Introduction, in this section we extend the VBEG model to the film geometry and study ^{3}He-^{4}He mixtures.

A. Model

We consider a three-dimensional slab of a simple cubic lattice consisting of $\bar{L}$ parallel (100) lattice layers with lattice spacing a so that $L = \bar{L}a$. Each layer has $\bar{A} = A/a^2$ sites, labeled $i, j, \ldots$, which are associated with an occupation variable $t_i = 0, 1$ and a phase θ_i ($0 \leq \theta_i < 2\pi$) which mimics the phase of the ^{4}He wave function and thus renders the XY bulk
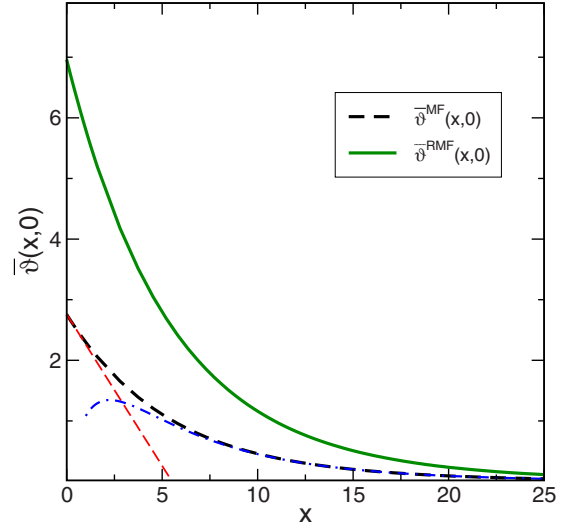

FIG. 2. (Color online) Dimensionless MF scaling function $\bar{\vartheta}^{MF}(x^{MF}, u_0 = 0) = f_C L^3 (v_0/90)^{1/2}$ [see Eq. (10)] with $x^{MF} = x = r_0 L^2$ plotted together with the renormalized mean-field scaling function $f_C L^3 = \bar{\vartheta}^{RMF}(x^{RMF}, 0)$ [see Eq. (33) and the main text] with $x^{RMF} = x = r L^2$ and $L/l_0 = 400$. $\bar{\vartheta}^{MF}(x^{MF} \to \infty, 0) \simeq 8(x^{MF})^{3/2} e^{-2(x^{MF})^{1/2}}$ (thin dash-dotted line) and $\bar{\vartheta}^{MF}(x^{MF} \to 0, 0) \simeq 2.76 - 0.5 x^{MF}$ (thin dashed line). The asymptotic behavior of $\bar{\vartheta}^{RMF}(x^{RMF}, 0)$ can be obtained from the one of $\bar{\vartheta}^{MF}(x^{MF}, 0)$ by multiplying the ordinate by the factor $[28/(8\pi^2/3)]^{1/2}[\ln(L/l_0)]^{1/2}$; the abscissa remains the same.

universality class ($n = 2$). A ^{3}He (^{4}He) atom at site i corresponds to $t_i = 0(1)$ so that in the bulk $X = 1 - \langle t_i \rangle$ is the ^{3}He concentration. Unoccupied sites are not allowed so that the model does not exhibit a vapor phase. Accordingly this model does not allow for the occurrence of a tricritical end point. However, we expect that the universal properties we are interested in are the same for tricritical points and tricritical end points. The Hamiltonian consists of bulk and surface contributions $\mathcal{H} = \mathcal{H}_b + \mathcal{H}_s$ with
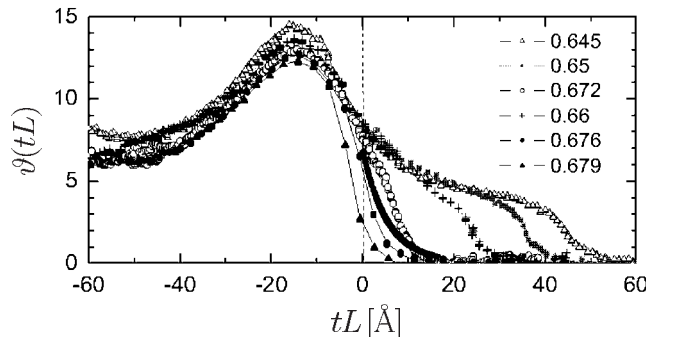

FIG. 3. Experimental data from Ref. [4] for the scaling functions $\vartheta = f_C L^3$ for the Casimir force in ^{3}He-^{4}He films of thicknesses L along various paths of fixed ^{3}He concentration (given in the figure) close to the tricritical concentration $X_t = 0.672$. The scaling variable is in units of Å. The solid line corresponds to the tricritical mean-field scaling function [4] calculated for $r_0 = 0$ [i.e., $a = 0$ in Eq. (15)] and suitably adjusted (see the main text); $t = (T - T_t)/T_t$.

$$\mathcal{H}_b = -J\sum_{\langle ij \rangle} t_i t_j \cos(\theta_i - \theta_j) - K\sum_{\langle ij \rangle} t_i t_j + \Delta \sum_i t_i, \quad (34)$$

where the first two sums run over nearest-neighbor pairs and the last one is over all lattice sites, except those at the surface. In this lattice gas model of ^{3}He-^{4}He binary mixtures the coupling constant K and the field Δ are related to the effective $^\alpha$He-$^\beta$He interactions $K_{\alpha\beta}$ (see, e.g., Ref. [27]),

$$K = K_{33} + K_{44} - 2K_{34}, \quad (35)$$

and to the chemical potentials μ_3 and μ_4 of ^{3}He and ^{4}He, respectively,

$$\Delta = \mu_3 - \mu_4 + 2q(K_{33} - K_{34}), \quad (36)$$

where q is the coordination number of the lattice ($q=2d$, where d is the spatial dimension of the system; $q=6$ in the present case). In the liquid the effective interactions $K_{\alpha\beta}$ are different for different α and β due to the differences in mass and of statistics between ^{3}He and ^{4}He atoms.

The properties of the model described by the bulk Hamiltonian $\mathcal{H}_b$ have been studied within MFT and by Monte Carlo simulations in $d=3$ [20]. In contrast to its two-dimensional version, for which there is no true tricritical point for any value of the model parameters, in $d=3$ for reasonable values of the interaction parameters the resulting phase diagram resembles that observed experimentally for ^{3}He-^{4}He mixtures, for which phase separation occurs as a consequence of the superfluid transition (see Fig. 4). The form of the surface Hamiltonian $\mathcal{H}_s$ should capture the phenomenon of superfluid film formation near a wall in ^{3}He-^{4}He mixtures [18] which generates an effective repulsion of ^{3}He atoms by the wall. The van der Waals interactions between the wall and ^{3}He or ^{4}He atoms are equal. However, ^{3}He atoms occupy a larger volume because of their larger zero-point motions. This gives rise to the preferential adsorption of ^{4}He atoms at the substrate-fluid interface, which may induce a local superfluid ordering and an enrichment of ^{3}He near the opposing fluid-vapor interface. Here we choose the following form for $\mathcal{H}_s$:

$$\mathcal{H}_s = \delta\Delta^{(l)} \overset{(l)}{\sum_i} t_i + \delta\Delta^{(r)} \overset{(r)}{\sum_i} t_i, \quad (37)$$

where the first sum runs over the sites of the first layer and the second over those in the Lth layer of the lattice. The differences $\delta\Delta^{(l)} \equiv \Delta^{(l)} - \Delta$ and $\delta\Delta^{(r)} \equiv \Delta^{(r)} - \Delta$ are measures of the relative preferences of ^{4}He atoms for the two surfaces such that $\delta\Delta^{(l)} < 0$ corresponds to the preference of ^{4}He atoms for the solid substrate.

B. Mean-field theory

We have studied the above model for the film geometry within mean-field theory. We have employed the variational method based on approximating the total equilibrium density distribution by a product of local site densities ρ_i (see, e.g., Ref. [28]). The corresponding variation theorem for the free energy reads
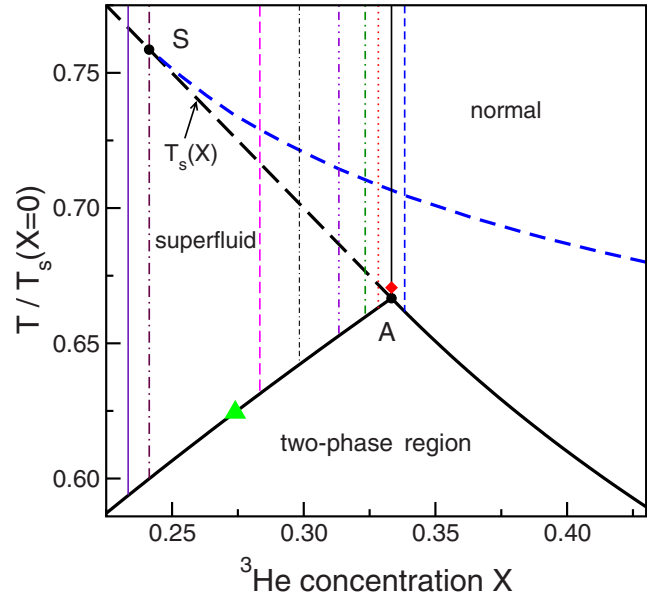

FIG. 4. (Color online) Bulk phase diagram for the VBEG model obtained within MFT for $K/J=0.5$ and $\Delta^{(l)}/J=-3$ exhibiting the line $T_s(X)$ of continuous superfluid transitions in the bulk (long-dashed line), the phase separation curves (solid lines), the tricritical point $A=(T_t/T_s(0)=2/3, X_t=1/3)$. In a semi-infinite system there is a (short-dashed) line of continuous surface transitions which merges with the line $T_s(X)$ of bulk critical points at the special transition point $S=(T_S/T_s(0)\simeq0.759, X_S\simeq0.241)$. Upon crossing this surface transition line a thin film near the surface becomes superfluid although the bulk remains a normal fluid. Vertical lines represent thermodynamic paths along which the Casimir force has been calculated (cf. Fig. 5). ◆, ● (A), ▲: state points which will be considered in Fig. 7.

$$F \le F_\rho = \text{Tr}(\rho \mathcal{H}) + (1/\beta)\text{Tr}(\rho \ln \rho), \quad (38)$$

where F is the exact free energy and F_ρ is an approximate free energy associated with the density distribution ρ; $\beta = 1/(k_B T)$. The minimum of F_ρ with respect to ρ subject to the constraint $\text{Tr}\rho=1$ is attained for the equilibrium density distribution $\rho = e^{-\beta\mathcal{H}}/\text{Tr}(e^{-\beta\mathcal{H}})$. Within mean-field theory the density distribution in the film geometry is approximated by

$$\rho = \rho_0 = \bar{A}^L \prod_{i=1}^{L} \rho_i, \quad (39)$$

i.e., the density distribution is constant within each layer parallel to the surfaces but varies from layer to layer. We treat the local layer density ρ_i as a variational ansatz, and the best functional form in terms of t_i and θ_i is obtained by minimizing $F_{\rho_0}/\bar{A} + \eta \, \text{Tr}(\rho_i)$ with respect to ρ_i and with η as a Lagrange multiplier in order to implement $\text{Tr}\,\rho=1$. This leads to

$$\rho_i = e^{-\beta h_i}/\text{Tr}(e^{-\beta h_i}), \quad (40)$$

where h_i is the single-layer mean field given by

$$h_i = -J(M_{i-1}^{(1)} + q_{\parallel}M_i^{(1)} + M_{i+1}^{(1)})t_i \cos \theta_i - J(M_{i-1}^{(2)} + M_{i+1}^{(2)})t_i \sin \theta_i - K(Q_{i-1} + q_{\parallel}Q_i + Q_{i+1})t_i + \Delta^{(i)}t_i, \quad (41)$$

where $\Delta^{(i)} = \Delta$ for $i \neq 1, \bar{L}$, and $\Delta^{(i)} = \Delta^{(l)}(\Delta^{(r)})$ for $i = 1(\bar{L})$. We have introduced the following order parameters:

$$Q_i \equiv 1 - X(i) = \mathrm{Tr}(t_i \rho_i) \quad (42)$$

and

$$M_i^{(1)} = \mathrm{Tr}(\rho_i t_i \cos \theta_i), \quad M_i^{(2)} = \mathrm{Tr}(\rho_i t_i \sin \theta_i). \quad (43)$$

$Q_i = \langle t_i \rangle$ corresponds to the concentration profile of ^{4}He, $X(i) = 1 - \langle t_i \rangle$ to the concentration profile of ^{3}He, and $M_i^{(1)}, M_i^{(2)}$ are the components of the two-component superfluid OP profile $\mathbf{M}_i$. $q_{\parallel}$ is the in-layer coordination number while each site (but not in the first and last layer) is connected to q' atoms in each adjacent layer and $q = q_{\parallel} + 2q'$ is the coordination number in the bulk of the lattice. Within our model $q' = 1$ and $q_{\parallel} = 2(d-1)$. This yields the following set of self-consistent equations for the OP $\mathbf{M}_i = (M_i^{(1)}, 0) \equiv (m_i, 0)$ in the ith layer:

$$Q_i = I_0(\beta Jb_i)/[e^{-\beta(Ka_i - \Delta^{(i)})} + I_0(\beta Jb_i)], \quad (44)$$

and

$$m_i = I_1(\beta Jb_i)/[e^{-\beta(Ka_i - \Delta^{(i)})} + I_0(\beta Jb_i)]. \quad (45)$$

$I_0(z)$ and $I_1(z)$ are the modified Bessel functions of the first kind, T is the temperature. We have introduced

$$b_i \equiv m_{i-1} + q_{\parallel}m_i + m_{i+1} \quad \text{for } i \neq 1, \bar{L}, \quad (46)$$

$b_1 \equiv q_{\parallel}m_1 + m_2$, and $b_{\bar{L}} \equiv m_{\bar{L}-1} + q_{\parallel}m_{\bar{L}}$, and analogously

$$a_i \equiv Q_{i-1} + q_{\parallel}Q_i + Q_{i+1} \quad \text{for } i \neq 1, \bar{L}, \quad (47)$$

$a_1 = q_{\parallel}Q_1 + Q_2$, and $a_{\bar{L}} = Q_{\bar{L}-1} + q_{\parallel}Q_{\bar{L}}$. The coupled sets of equations for Q_i and m_i are solved numerically by standard methods of multidimensional root finding. The equilibrium solution minimizes the free energy per number of lateral lattice sites $\mathcal{F} \equiv F_{\rho_0}/\bar{A}$:

$$f = \sum_{i=2}^{\bar{L}-1} \left(\frac{J}{2}(m_{i-1}m_i + q_{\parallel}m_i^2 + m_{i+1}m_i) + \frac{K}{2}(Q_{i-1}Q_i + q_{\parallel}Q_i^2 \right.$$
$$\left. + Q_{i+1}Q_i) \right) + k_B T \sum_{i=1}^{\bar{L}} \ln(1 - Q_i) + f_1 + f_2, \quad (48)$$

where

$$f_1 = \frac{J}{2}(q_{\parallel}m_1^2 + m_2 m_1) + \frac{K}{2}(q_{\parallel}Q_1^2 + Q_2 Q_1) \quad (49)$$

and

$$f_2 = \frac{J}{2}(m_{\bar{L}-1}m_{\bar{L}} + q_{\parallel}m_{\bar{L}}^2) + \frac{K}{2}(Q_{\bar{L}-1}Q_{\bar{L}} + q_{\parallel}Q_{\bar{L}}^2). \quad (50)$$

The above equations neglect the helicity, i.e., $\mathbf{M}_i = (M_i^{(1)}, 0) \equiv (m_i, 0)$. In general the helicity might be nonzero because
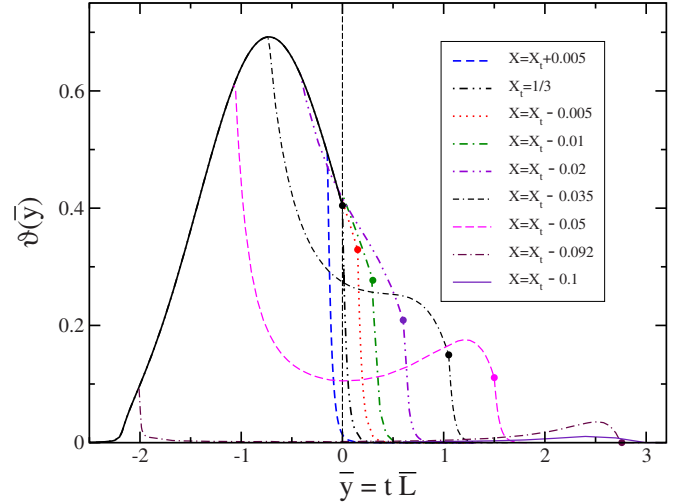

FIG. 5. (Color online) Dimensionless scaling function $\vartheta(\bar{y} = t\bar{L}) = f_C \bar{L}^3$, with $t = (T - T_t)/T_t$ and $\bar{L} = 20$ for the Casimir force calculated within MFT for the VBEG model along the paths of fixed concentration of ^{3}He shown in Fig. 4. Dots indicate the corresponding onset temperature $T_s(X)$ of superfluidity at the line of bulk critical points. The full line for $\bar{y} < 0$ corresponds to the temperatures of the onset of the first-order phase separation in the bulk (see Fig. 4). In view of, cf., Fig. 9 we note that the curves might still shift if calculated for larger values of $\bar{L}$.

the BCs for the superfluid OP are effectively nonsymmetric, i.e., $\mathbf{M}_1 \neq 0$ whereas $\mathbf{M}_L = 0$ so that the superfluid OP can in principle rotate across the film. The relevance of the helicity on the Casimir force will be analyzed elsewhere.

C. Results for ^{3}He-^{4}He mixtures

First, we have analyzed the semi-infinite system. Close to the line of *bulk* critical points we have found a higher ^{4}He concentration near the surface (chosen to be the left side of the system), which induces a local superfluid ordering. By varying T and Δ one obtains a line of continuous *surface* transitions corresponding to the onset of the formation of this superfluid film near the wall; it meets the line of bulk critical points at a so-called special transition point, the position of which depends on the value of $\Delta^{(l)}$ (see Fig. 4). These findings are in agreement with the results of a Migdal-Kadanoff analysis [29].

In the film geometry the Casimir force f_C [Eq. (2)] is obtained by calculating $f^{ex}(\bar{L})$ [see Eq. (3)] for $\bar{L}$ and $\bar{L}+1$ and taking the difference. [Note that in the lattice model f is the total free energy of the film per number $\bar{L}\bar{A}$ of lattice sites and f_b is the bulk free energy density per $\bar{L}\bar{A}$. Accordingly $f^{ex}(\bar{L}) = (f - f_b)\bar{L}/(k_B T_t)$, $f_C = -\partial f^{ex}/\partial \bar{L}$, as well as $\vartheta = f_C \bar{L}^d$ with $d = 3$ near tricriticality and $d = 4$ near the λ transition are dimensionless. In order to avoid a clumsy notation we do not introduce different symbols for the lattice and the continuum versions of the free energies.] Figure 5 summarizes our result for a film of thickness $\bar{L} = 20$, $K/J = 0.5$, $\Delta^{(l)}/J = -3$, and $\Delta^{(r)} = \Delta_t/J \simeq 0.61$, which is the tricritical bulk value. Such a

choice of the surface coupling constants corresponds to non-symmetric BCs and is consistent with the assumption made in Ref. [4] for the concentration profile across the wetting film, whereupon at the interface with the vapor the ^{3}He concentration takes the bulk value. For temperatures above the bulk coexistence line at first-order demixing transitions f_C is calculated along the thermodynamic paths indicated in Fig. 4 which correspond to fixed ^{3}He concentrations X. Our selection of X covers the tricritical region as well as the crossover to the critical superfluid behavior of pure ^{4}He, i.e., $X=0$. In order to calculate the force at a fixed value X_0 we first determine $\Delta(X=X_0,T)$ by solving the two coupled self-consistent equations for $Q(\Delta,T)=1-X$ and $M(\Delta,T)$ in the bulk [Eqs. (12) and (13) in Ref. [20]]. For each temperature along the thermodynamic paths indicated in Fig. 4 we solve Eqs. (44) and (45) with this value $\Delta(X=X_0,T)$. This renders the profiles $Q(l)$ and $m(l)$ and allows us to calculate the free energy from Eq. (48). When upon lowering the temperature the paths of constant X reach the coexistence line of two-phase coexistence (see Fig. 4) we continue our calculations along the coexistence line, infinitesimally on the superfluid branch of bulk coexistence. In Fig. 5 this leads to the full line for $T<T_t$, i.e., $y<0$.

Contrary to the LG model, for the present microscopic model it is natural to express the properties of the system as functions of the experimental thermodynamic fields t and $(\Delta-\Delta_t)/(k_B T_t)$ or the scaling fields t and g [see Eq. (17)]. Accordingly, we present our results for the Casimir force in terms of the scaling function defined through the relation $\vartheta \equiv \bar{L}^3 f_C$ as a function of only a single scaling variable $\bar{y} \equiv t\bar{L}^{1/\nu} = [(L/a)/(\xi/\xi_0^+)]^{1/\nu}$. $\xi_0^+ = \bar{\xi}_0^+ a$ is the amplitude of the order parameter correlation length $\xi = \xi_0^+ t^{-\nu} = \bar{\xi} a$ above T_t and $\nu(d=3)=1$. The second relevant scaling variable $x \equiv g\bar{L}^2$ also varies along a path of fixed ^{3}He concentration (see Fig. 6) and a proper scaling description has to account for it. However, in order to be able to compare our results with the presentation of the corresponding experimental ones [4], we follow Ref. [4] where the variation of x has been neglected. As can be inferred from the phase diagram in Fig. 6, the g components of the paths $X=$const in the phase diagram are smaller than the t components, so that the form of the scaling function for these paths are expected be close to $\vartheta(x=0,y)$. Also experimentally the variation of the scaling variable g along the path of fixed X cannot be determined easily.

Near the tricritical point paths of constant X cross three different phase transition lines: the surface transition line, the line of bulk critical points, and the line of first-order phase coexistence. As shown in Fig. 5, close to the surface transition f_C is small and this transition does not leave a visible trace in its behavior. f_C remains small up to the coexistence line or to the line of bulk critical points for $X>X_t$ or $X<X_t$, respectively. There it increases very steeply and for ^{3}He concentrations $X<X_t$ upon crossing the line of bulk critical points there is a break in slope (see the dots in Fig. 5) giving rise to the formation of shoulders which are similar to those observed experimentally [4]. When T reaches the temperature of first-order phase separation, f_C is given by the curve (full line for $y<0$ in Fig. 5) common to all values of
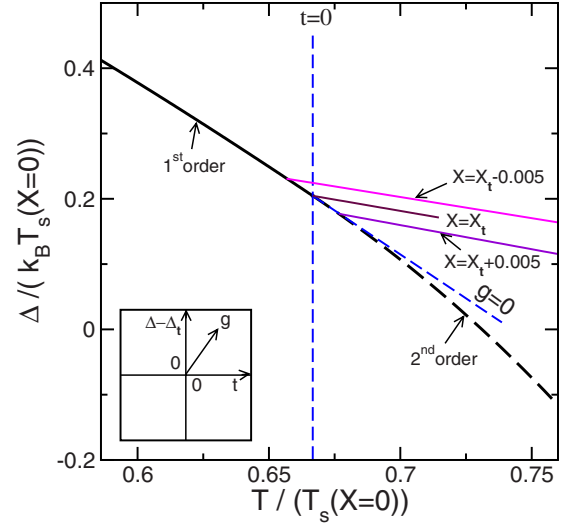

FIG. 6. (Color online) Bulk phase diagram for the VBEG model in the (Δ,T) plane obtained within MFT for the same set of parameters as in Fig. 4. The long-dashed coexistence line corresponds to the continuous superfluid transitions whereas the solid coexistence line corresponds to the curve of first-order phase separation. As indicated in the inset g and t are the two relevant scaling variables [compare Eq. (17)]; the line $g=0$ is tangential to the coexistence line at the tricritical point where the lines of first- and second-order transitions merge. Note that according to Eq. (17) along the line $g=0$ one has $(\Delta-\Delta_t)/(k_B T_t)=-a't$ and along the line $t=0$ one has $g=(\Delta-\Delta_t)/(k_B T_t)$. Three thermodynamic paths of constant concentration are shown: $X=X_t$, $X=X_t-0.005$ (upper line), and $X=X_t+0.005$ (lower line). We note that along the paths of constant concentration both scaling variable t and g vary; however, the variation of t is more pronounced so that within a rough approximation g can be considered to be constant along each path.

X. These curves of constant X meet the full line with different slopes.

The aforementioned common curve exhibits a pronounced maximum below T_t at $y\simeq-0.74$ and gradually decreases to zero for $y\rightarrow-\infty$. The properties of the Casimir force in this temperature region can be attributed to purely interfacial effects. Indeed, we observe that below T_t both the concentration and the superfluid OP profile corresponding to this common curve display an interfacelike structure separating two domains of the coexisting bulk phases (see the case $t=-0.0633$ in Fig. 7). This film phase is soft with respect to shifts of the interface position and is similar to the one occurring in Ising-like films with opposite BCs [30] for temperatures below the bulk critical temperature but above the wetting temperature of the confining walls, in which case the Casimir force is repulsive with a pronounced maximum occurring below the bulk critical temperature [31]. In general a positive sign of the force can be regarded as a consequence of entropic repulsion [32]. Typically the maximum of the force occurs at that temperature T at which the interfacial width, which is proportional to the bulk correlation length ξ of the order parameter, becomes comparable with the width L of the film. In the present case both the concentration and the superfluid OP profile contribute to the free energy and hence to the Casimir force. Their interfacial widths are pro-
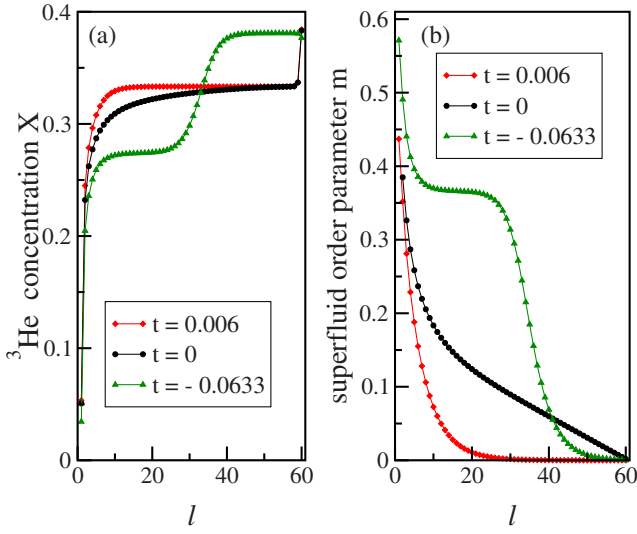
FIG. 7. (Color online) (a) ^{3}He concentration profile $X(l)=1-Q_l$ and (b) superfluid OP profile m_l for a VBEG film of thickness $\bar{L}=60$ for $K=0.5J$, $\Delta^{(l)}/J=-3$, and $\Delta^{(r)}/J=\Delta_t/J\simeq0.61$ corresponding to the state points ◆, ●, and ▲ indicated in Fig. 4; $t=(T-T_t)/T_t$.

FIG. 8. (Color online) (a) ^{3}He concentration profile $X(l)=1-Q_l$ and (b) superfluid OP profile m_l for a VBEG film of width $\bar{L}=60$ for $K=0.5J$, $\Delta^{(l)}/J=-\infty$, and $\Delta^{(r)}/J=+\infty$ corresponding to the state points ◆, ●, and ▲ indicated in Fig. 4 with $t=(T-T_t)/T_t$.

portional to correlation length ζ associated with concentration fluctuations and to the OP correlation length ξ, respectively. As can be seen from Figs. 7 and 8, within MFT these interfacial widths and therefore ζ and ξ are comparable. Accordingly, by analogy with Ising-like systems [30] we expect that within MFT the maximum of the force occurs when ξ (or, equivalently, $\zeta\simeq\xi$) is of the order of L, which is actually consistent with what is observed in Fig. 5, where the maximum of the scaling function is located at $y\simeq-1$. We may expect that also in the actual system the occurrence of the maximum of the Casimir force below the tricritical point can be attributed to such interfacial effects. However, since the correlation length of the superfluid OP $\xi=\infty$ in the superfluid phase it is not yet clear which length scale governs the interfacial width of the superfluid OP profile in the "soft mode" phase below T_t and hence what length scale determines the position of the force maximum.

For $X\lesssim X_t-0.05$ we observe a crossover to the critical superfluid behavior of pure ^{4}He and a gradual formation of a second, less pronounced local maximum located slightly below the line of bulk critical points ($y>0$ in Fig. 5). This local maximum decreases upon departing from X_t and finally f_C becomes vanishingly small along paths which cross the line of bulk critical points above the special transition S (see Fig. 4). This is expected, because above S there is no longer a superfluid film formation near the solid substrate for thermodynamic states corresponding to the bulk "normal" phase of a fluid close to the line of bulk critical points. This means that the superfluid OP in the film is identically zero up to the line of bulk critical points and the BC effectively turn into the type (O,O) for which f_C vanishes within MFT. [For (O,O) BC fluctuations beyond MFT generate an attractive Casimir force $f_C<0$ [10].] For lower T, f_C increases steeply upon approaching bulk coexistence revealing that interfacial effects associated with the soft mode lead to a much stronger
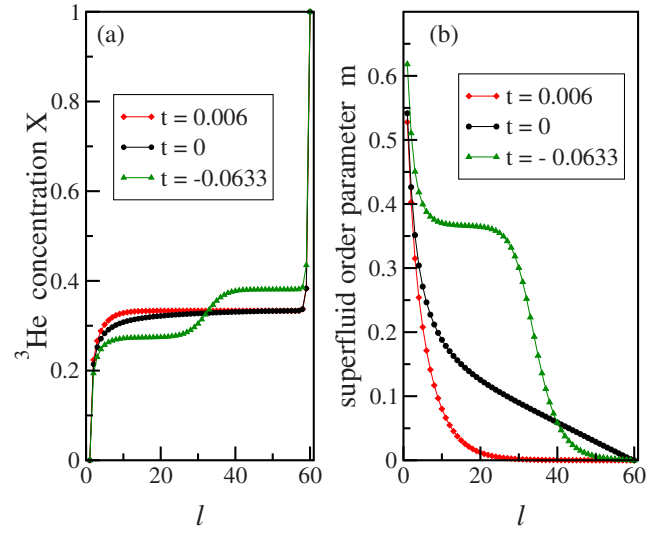
Casimir effect than the critical fluctuations near the line of bulk critical points.

IV. RESULTS FOR PURE ^{4}He

A. The limiting case of the VBEG model

In this section we consider the limiting case $\Delta\to-\infty$ in which all lattice sites are occupied, i.e., $t_i\to1$. In this case the first term of the bulk Hamiltonian $\mathcal{H}_b$ in Eq. (34) corresponds to the classical XY model (the planar rotator model) for pure ^{4}He and therefore, as far as the bulk contribution is concerned, the partition function of the VBEG model reduces to that of the XY model up to a factor e^{KzN} where N is the number of lattice sites. The corresponding MFT equations for the bulk OP can be inferred from Eqs. (44) and (45) with $m_i\equiv M$ yielding

$$Q=1, \quad M=\frac{I_1(\beta qJM)}{I_0(\beta qJM)} \tag{51}$$

for temperatures below the bulk superfluid transition, which is located at $T_s(X=0)=T_\lambda=qJ/2$, and $Q=1$, $M=0$ above $T_\lambda=T_s(X=0)$. The scaling behavior of the free energy and of the Casimir force close to this critical point (see below) is consistent with an upper critical spatial dimension $d^*=4$. The crossover to the tricritical behavior with $d^*=3$ and with tricritical exponents occurs only upon approaching the tricritical point $A=[T_t/T_s(0)=2/3, X_t=1/3]$ (see Fig. 4).

In the slab geometry we take also the limits $\Delta^{(l)}$, $\Delta^{(r)}\to-\infty$ which, together with the absence of external fields coupling to the superfluid OP, lead to the (O,O) BC for the superfluid OP. Thus this limiting case allows us to study the Casimir force for wetting films of pure ^{4}He near the superfluid transition at $T_c=T_\lambda$. We remark that in the slab geometry the superfluid transition is actually of the Kosterlitz-

Thouless type [33]. However, this change of the character of the transition is not captured by MFT. The corresponding set of equations for the superfluid OP in the lth layer of the slab is

$$m_l = \frac{I_1(\beta J b_l)}{I_0(\beta J b_l)}, \quad b_l \equiv m_{l-1} + q_\| m_l + m_{l+1} \quad \text{for} \quad l \neq 1, \bar{L},$$

$$(52)$$

where $b_1 \equiv q_\| m_1 + m_2$ and $b_{\bar{L}}^- \equiv m_{\bar{L}-1}^- + q_\| m_{\bar{L}}^-$. The equilibrium free energy divided by the number A of lattice sites within one layer takes the form

$$f = \sum_{l=2}^{\bar{L}-1} \left[\frac{J}{2} (m_{l-1} m_l + q_\| m_l^2 + m_{l+1} m_l) \right] + \frac{J}{2} (q_\| m_1^2 + m_2 m_1)$$

$$+ \frac{J}{2} (m_{\bar{L}-1}^- m_{\bar{L}}^- + q_\| m_{\bar{L}}^2) + k_B T \sum_{l=1}^{\bar{L}} \ln[I_0(\beta J b_l)], \quad (53)$$

where m_l, $l = 1, \ldots, \bar{L}$, are the solutions of Eq. (52). Solving Eq. (52) for different widths of the film we have found that the superfluid OP profile vanishes for temperatures larger than a certain $T_c(\bar{L}) < T_s(X=0) = T_\lambda$ which can be identified with the critical temperature $T_c(\bar{L})$ of the slabs. Below $T_c(\bar{L})$ the corresponding Casimir force turns out to be negative (i.e., attractive) as expected for the (O,O) BC pertinent to the case of pure ^{4}He. The lattice calculations have been carried out for $d=3$ and are presented in terms of the scaling function $\vartheta_0(y = \tau(L/\xi_0^+)^2) \equiv \bar{L}^d f_C$ with $d=4$ in accordance with MFT and $\tau \equiv (T-T_\lambda)/T_\lambda$. Within lattice MFT the actual space dimensionality d of the lattice does not influence the shape of the scaling function in the scaling limit $\xi(\tau > 0) = \xi_0^+ \tau^{-\nu} \gg a$; indeed, it enters only into the nonuniversal amplitude ξ_0^+ via the ratio $q'/q = (2d)^{-1}$ between the bulk interlayer and the total site coordination numbers q' and q, respectively. ϑ_0 has been calculated for $\bar{L} = 20$, 40, and 60 and is plotted in Fig. 9 as a function of $y \equiv \tau(L/\xi_0^+)^{1/\nu}$ with the MFT value $\nu = 1/2$. Exploiting the fact that within MFT $\xi(\tau < 0)$ is finite we have determined the amplitude ξ_0^- of the correlation length $\xi(\tau < 0) = \xi_0^-(-\tau)^{-\nu}$ from the exponential approach of the OP profiles towards the corresponding bulk values m_b which are actually attained in the middle of the film (see Fig. 10) at temperatures sufficiently below $T_s(X=0)$ (see, e.g., Fig. 21 in Ref. [34]). The MFT universal amplitude ratio $\xi_0^+/\xi_0^- = \sqrt{2}$ then yields the estimate $\bar{\xi}_0^+ \simeq 0.41$ for the VBEG model on the lattice. We emphasize here that scaling of the force data occurs only for surprisingly thick films, i.e., $\bar{L} \gtrsim 60$, as revealed clearly by the analysis presented in the next subsection.

B. Comparison with the Landau-Ginzburg theory

In Ref. [34] within MFT for the $O(2)$ LG continuum theory [see Eq. (1) with $v_0 = 0$] the order parameter profiles $\Phi = (m(z), 0)$ in a slab with the (O,O) BC have been calculated analytically [see Eqs. (202) and (203) in Appendix D in Ref. [34]]. It turns out that as a function of the scaling vari-
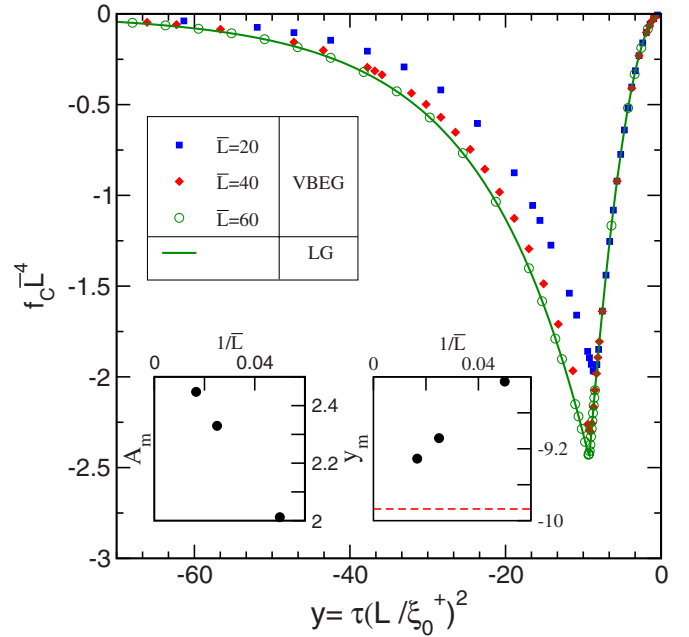

FIG. 9. (Color online) Mean-field scaling function $\vartheta_0(y = \tau(L/\xi_0^+)^2) = f_C \bar{L}^4$ for the limiting case of the VBEG model (symbols) corresponding to pure ^{4}He and various film thicknesses $\bar{L}$ with $\tau = (T-T_\lambda)/T_\lambda$. The full curve corresponds to the scaling function $\vartheta_0^{LG}(y)$ obtained from the continuum $O(2)$ LG theory within MFT [Eqs. (55) and (56)] with the amplitude $A_m = A_m(\bar{L})$ and the position of the minimum $y_m = y_m(\bar{L})$ determined in such a way as to provide the best fit to ϑ_0 from the VBEG model; for further details see the main text. With this rescaling the continuum theory provides a very good fit (here shown only for $\bar{L} = 60$) to the numerical data. The insets show the $\bar{L}$ dependence of A_m and y_m used as fitting parameters. The dashed line in the inset for $y_m(\bar{L})$ indicates the limiting value $y_m = -\pi^2$ predicted by th LG model. Surprisingly, scaling—corresponding to $\bar{L}$-independent A_m and y_m—is not yet attained by the numerical data of the VBEG model even for thick slabs with $\bar{L} \simeq 60$.

able $y = \tau(L/\xi_0^+)^{1/\nu} = r_0 L^2$ [where $r_0 \propto \tau$ is the coefficient appearing in Eq. (1)] the mean-field OP profile $m(z)$ vanishes for $y \geq y_m \equiv -\pi^2$, whereas it is nontrivial for $y < y_m$, breaking the original $O(2)$ symmetry. This occurs for temperatures below the shifted critical point of the film which therefore corresponds to $y = y_m$ (see Ref. [35]). In Fig. 10 we compare the OP profiles (normalized by the corresponding bulk values as to obtain universal scaling functions of y and z/L) calculated within the VBEG model (for a lattice with $\bar{L} = 150$) and within LG continuum theory for a selection of values of the scaling variable y. The agreement between the profiles is very good, although the VBEG profiles exhibit a slight asymmetry with respect to $z/L = 1/2$ which is due to the limited numerical accuracy of the lattice calculation.

The knowledge of the analytic expression for $m(z)$ allows one to compute the stress tensor [Eq. (4)] as a function of the scaling variable y:
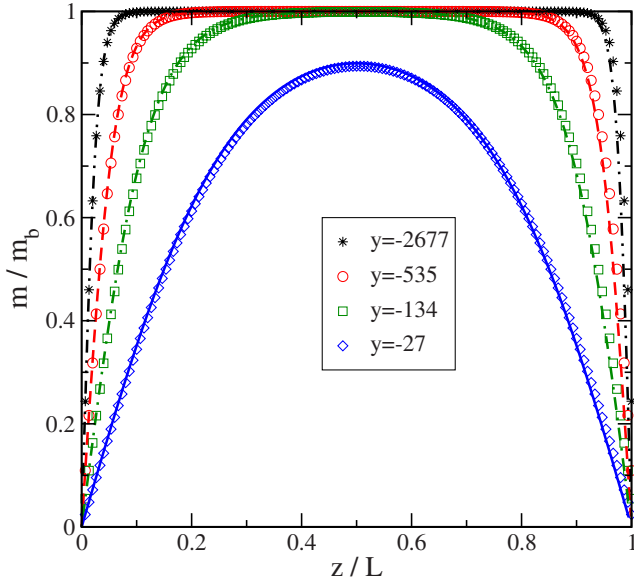
FIG. 10. (Color online) Mean-field OP profiles (normalized to the corresponding bulk values m_b) across slabs of thickness L calculated from the limiting case of the VBEG model (symbols, $\bar{L}$ =150) and from the continuum $O(2)$ LG theory [lines, see Eqs. (202) and (203) in Ref. [34]] for a selection of the scaling variable $y=\tau(L/\xi_0^+)^{1/\nu}$ below the shifted critical point of the film (corresponding to $y=y_m=-\pi^2$, see the main text). For y sufficiently negative $m(z\gg a)-m_b\sim\exp[-z/\xi(\tau<0)]$ in the middle of the slab. This allows one to infer $\bar{\xi}_0=\bar{\xi}(\tau<0)(-\tau)^{1/2}\simeq0.29$ so that $\bar{\xi}_0^+=\sqrt{2}\bar{\xi}_0$ $\simeq0.41$.

$$\mathcal{T}_{zz} = \frac{1}{2}[m'(z=0)]^2$$

$$= \begin{cases} \dfrac{A_m}{L^4}\dfrac{4k^2}{(1+k^2)^2}\left(\dfrac{y}{y_m}\right)^2, & \text{for } y < y_m = -\pi^2, \\ 0, & \text{for } y \geq y_m, \end{cases}$$

$$(54)$$

where $A_m=3\pi^4/(2u_0)$ and $k=k(y<y_m)$ is the real solution of the implicit equation

$$\frac{y}{y_m} = \frac{4}{\pi^2}(1+k^2)K^2(k),\quad\quad (55)$$

where $K(k)$ is the complete elliptic integral of the first kind, such that $k(y=y_m)=0$ and $k(y\to-\infty)=1$. The stress tensor $\mathcal{T}_{zz,b}$ in the bulk, related to the *bulk* free energy density $f_b(\tau)$, can be obtained from Eq. (54) in the limit $L\to\infty$ at fixed reduced temperature τ, yielding $\mathcal{T}_{zz,b}(\tau<0)=A_mL^{-4}(y/y_m)^2$ (which is actually independent of L due to $y\propto\tau L^2$) and $\mathcal{T}_{zz,b}(\tau>0)=0$. Accordingly, the Casimir force f_C per unit area of the cross section of the film and in units of k_BT_λ is given by $f_C=\mathcal{T}_{zz}-\mathcal{T}_{zz,b}$ and its scaling function $\vartheta_0^{LG}=L^4f_C$ can be derived from the expressions for $\mathcal{T}_{zz}$ and $\mathcal{T}_{zz,b}$ discussed above:

$$\vartheta_0^{LG}(y) = \begin{cases} -A_m\left(\dfrac{1-k^2}{1+k^2}\right)^2\left(\dfrac{y}{y_m}\right)^2 & \text{for } y < y_m = -\pi^2, \\ -A_m\left(\dfrac{y}{y_m}\right)^2 & \text{for } y_m \leq y < 0, \\ 0 & \text{for } y \geq 0. \end{cases}$$

$$(56)$$

The independent calculation of $\vartheta_0^{LG}(y)$, recently presented in Ref. [36], agrees with this expression. At $y=y_m=-\pi^2$ the scaling function (56) exhibits a cusp singularity at which it attains its minimum value $\vartheta_{\min}^{LG}\equiv\vartheta_0^{LG}(y_m)=-A_m<0$ where A_m is given after Eq. (54). Within MFT the coupling constant u_0 and therefore A_m remain undetermined. In order to compare the LG result with the VBEG results, accounting also for corrections due to the finite size $\bar{L}$ of the latter, we introduce an adjusted scaling function $\bar{\vartheta}_0^{LG}(y)$ which is given by Eq. (56) with $A_m=A_m(\bar{L})$ and $y_m=y_m(\bar{L})$ determined by a best fit to the VBEG scaling function $\vartheta_0(y)$ calculated for lattices with $\bar{L}=20$, 40, and 60. For all values of $\bar{L}$ considered, $\bar{\vartheta}_0^{LG}(y)$ provides a very good fit to the numerical data, as demonstrated in Fig. 9 for $\bar{L}=60$. In the inset of Fig. 9 we plot the functions $A_m(\bar{L})$ and $y_m(\bar{L})$ obtained from the fit. According to the results of the LG theory one expects $y_m(\bar{L}\to\infty)=-\pi^2\simeq-9.87$ (which is represented as a solid line in the inset), and indeed the results of the VBEG model show the correct trend, although finite-$\bar{L}$ corrections are still present even for the largest lattice $\bar{L}=60$ considered here, with $y_m(\bar{L}=60)\simeq-9.31$. The amplitude $A_m(\bar{L})$ shows even stronger corrections and indeed the value $A_m(\bar{L}=60)\simeq2.45$ might underestimate the actual asymptotic value by $15-20$ %.

Beyond MFT the renormalized coupling constant u attains its fixed-point value under RG flow which fixes the amplitude A_m and the magnitude of the corrections to the scaling functions. This would then allow a complete numerical test with the scaling function ϑ_0 of the VBEG model as obtained, e.g., from Monte Carlo simulations. In Ref. [36] the amplitude $A_m=3\pi^4/(2u_0)$ [see the text after Eq. (54)] has been estimated beyond MFT by replacing u_0 by the fixed-point value u^* calculated within field theory. Although this approach provides a theoretical estimate for $(A_m)_{theo}=6.92$, it fails in accounting quantitatively for the actual amplitude $(A_m)_{exp}=1.30\pm0.03$ observed in experiments [7].

For a given film thickness L, the position of the minimum of the scaling function corresponds to the reduced critical temperature $\tau_m(L)=[T_c(L)-T_\lambda]/T_\lambda=y_m(\xi_0^+/L)^{1/\nu}$ which reflects the onset temperature $T_c(L)<T_c(L=\infty)=T_\lambda$ for superfluidity in the slab. For $\tau>\tau_m$ the superfluid OP profile vanishes and so does the mean-field free energy of the film. Thus from Eqs. (2) and (3) it follows that for $T>T_c(L)$ one has $L^df_C=-L^df_b/(k_BT_\lambda)\sim-L^d\tau^{2-\alpha}=-(\tau L^{1/\nu})^{d\nu}$, using the hyperscaling relation $2-\alpha=d\nu$. For $d=4$ and $\nu=1/2$ this implies that $\vartheta_0(y_m<y<0)\sim y^2$ (for $y>0$, within MFT $f_b=0$ and therefore $f_C=0$) which agrees with Eq. (56).

V. DISCUSSION OF THE RESULTS OBTAINED FROM THE VBEG MODEL

A. ^{3}He-^{4}He mixtures

As one can infer from the comparison of Figs. 5 and 3 the qualitative features of the scaling functions ϑ for ^{3}He-^{4}He mixtures extracted from the experimental data for $X \simeq X_t$, such as the sign of the force, the occurrence of the pronounced maximum below T_t, and the formation of shoulders above T_t, are well captured by the present lattice model. The breaks in slopes upon crossing the λ line shown in Fig. 5 are features of the mean-field approach and are expected to be smeared out by fluctuations.

The experimental data for the Casimir force f_C exhibit a maximum at $tL \simeq -18$ Å which cannot be related to the condition $\xi \sim \zeta \sim L$ borne out by the mean-field analysis (Fig. 5) because actually, i.e., beyond MFT, $\xi = \infty$ in the superfluid phase. Further studies are needed to determine what length scale governs the interfacial width of the superfluid OP profile in the soft mode phase below T_t. This analysis, which is left to future research, has to take into account that the actual width of the interface formed in the film (see, e.g., the case $t = -0.0633$ in Fig. 7), is broadened both by the Goldstone modes in the superfluid phase and by capillary-wave like fluctuation.

Different from the mean-field scaling function ϑ the experimental one does not vanish at low temperatures, which is expected to be due to the aforementioned Goldstone modes of the broken continuous symmetry in the superfluid phase and due to helium-specific [15] surface induced fluctuations which both evade the present mean-field analysis. A similar behavior has been found in wetting experiments for pure ^{4}He films near the λ line [2], in which the film thicknesses above and below the λ transition are not the same, so that the wetting films are thinner in the superfluid phase. For pure ^{4}He, Zandi *et al.* [15] pointed out that the Goldstone modes indeed lead to thinner superfluid films for $T \ll T_c$. But this estimate is not applicable for $T \approx T_\lambda$ and for $T \ll T_\lambda$ it is too small to account for the experimentally observed magnitude of the thinning. This view of the effect of the Goldstone modes on ϑ is supported by Monte Carlo simulation data for the XY model with periodic BCs [37]. The capillary wavelike surface fluctuations, which occur on one of the bounding surface of the superfluid ^{4}He wetting film, give rise to an additional force (similar in form but larger in magnitude) which may then together explain the experimental observation [15,38].

For a mixture, however, it is possible that the apparent thickening of a wetting film as inferred from capacity measurements might be, at least partially, an artifact due to a significant change of the permittivity within the film [39]. Upon inferring the film thickness from the permittivity, in Ref. [4] it was assumed that $X_{film} = X_t$ which does not hold at low temperatures at which the soft mode occurs. In order to estimate the error the assumption $X_{film} = X_t$ introduces into the determination of the film thickness L we repeat the calculation for determining L by taking into account the interfacelike *concentration* profile below T_t (see Fig. 7) and by assuming a mean-field-like shape:

$$X(z) = \frac{1}{2}(X^I + X^{II}) - \frac{1}{2}(X^I - X^{II})\tanh[(z - z_0)/(2\zeta)],$$

$$(57)$$

where X^I and X^{II} are the concentrations of the coexisting bulk phases (see the triangle in Fig. 4), $z_0 = L/2$ is the position of the center of the interface, and ζ is the correlation length associated with concentration fluctuations. We note that ζ is finite in the superfluid phase whereas $\xi = \infty$ for the superfluid OP. The effective permittivity constant $\bar{\epsilon}_{film}$ of the film follows from adding in series the capacitance C for each slice of the film and from using $C \sim \epsilon$ [4]:

$$\bar{\epsilon}_{film}(X, T) = \frac{L}{\displaystyle\int_0^L dz/\epsilon(z)},$$

$$(58)$$

where $\epsilon(z)$ is related to the concentration profile via [40]

$$\epsilon(z) - 1 = [5.697 - 1.402X(z)] \times 10^{-2}. \quad (59)$$

From this we have found that neglecting at low temperatures the variation of the concentration across the film introduces an error in the determination of its thickness from capacity measurements (leading indeed to an increased film thickness) which is about 35% of the 40 Å difference in thickness reported above and below T_t. Specifically, at $T = 0.65$ K the bulk concentrations are $X^I = 0.325$, $X^{II} = 0.825$, and the bulk correlation length is $\zeta = \zeta_0 |t|^{-1} \approx 5.1$ Å, where following Ref. [4] we have assumed $\zeta_0 = 1.3$ Å as the value measured for concentration fluctuations far below T_t in the superfluid phase. Accordingly, approximating the actual inhomogeneous permittivity by the homogeneous one gives rise to an error ≈ 14 Å.

In the crossover regime along the line of critical points connecting the tricritical point and the critical λ transition in pure ^{4}He only few experimental data for the thicknesses of the wetting films are published. Nonetheless, the observed variations of film thicknesses there again agree with the present theoretical findings for the Casimir force. In particular, one observes a rapid thickening of the films upon approaching the line of bulk critical points; for specific values of X a small maximum located slightly below the line of bulk critical points is also visible (compare Fig. 5).

Two reasons impede a more quantitative comparison of our results obtained within the VBEG model with the experimental ones. First, for our choice of surface terms in the Hamiltonian the fixed-point BC $(+, O)$ for the order parameter cannot be realized within the VBEG model. Taking the limits $\Delta_1 \to -\infty$ and $\Delta_2 \to \infty$ in Eqs. (44) and (45) assures that $X(1) = 0$ and $X(\bar{L}) = 1$. However, even this limiting concentration profile does not induce the required BC: although $m(\bar{L}) = 0$ one has $m(1) = I_1(\beta J b_1)/I_0(\beta J b_1) \neq 1$, i.e., the superfluid OP at the solid substrate is never saturated at its maximum value 1 which corresponds to the BC $(+)$ (see Fig. 8). We have checked that in this limiting case with respect to $\Delta_{1,2}$ the qualitative behavior of the Casimir force is the same; only the magnitude of f_C is slightly bigger [$\vartheta(0) \approx 0.5$ for the limiting case, whereas $\vartheta(0) \approx 0.4$ for the case shown in Fig.
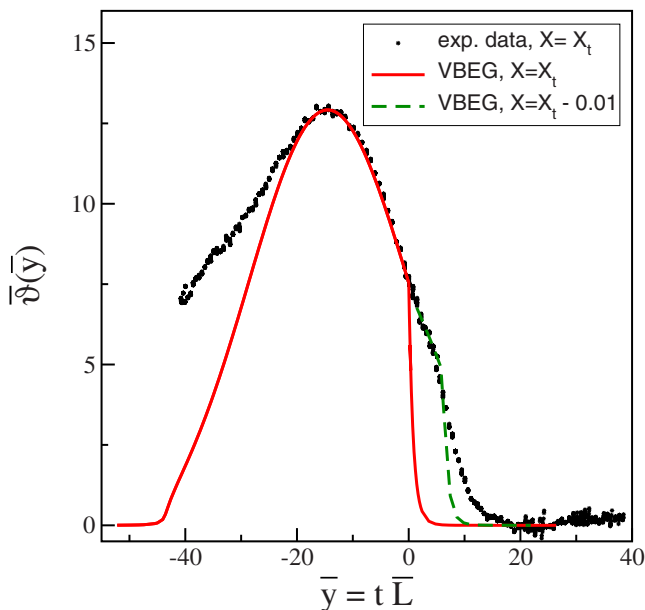
FIG. 11. (Color online) The adjusted scaling function $\bar{\vartheta}(\bar{y})$ (see the main text) for the VBEG model within MFT compared with the corresponding experimental curve [4] obtained along the path of fixed tricritical concentration $X=X_t \approx 0.672$ of ^{3}He. $\bar{\vartheta}(\bar{y})$ is obtained from $\vartheta(\bar{y})$ in Fig. 5 by rescaling the amplitudes of ϑ and $\bar{y}$ such that there is agreement between the experimental data for $X=0.672$ at $\bar{y}=0$ and with respect to the positions of the maximum. The VBEG curve for $X=X_t-0.01$ agrees with the experimental data for nominally $X=X_t$ even better. Both theoretical curves coincide for $\bar{y}<0$.

5]. In order to be able to extract universal properties—which requires us to reach the fixed-point BC—it would be necessary to introduce a surface field which couples directly to the superfluid OP so that the BC (+) can be realized; but such a surface field has no physical basis. Finally, even at the upper critical dimension $d=d^*=3$ due to logarithmic corrections our present MFT is not sufficient. However, a naive correction of ϑ obtained within the VBEG model by multiplying it by the logarithmic factor $[\ln(L/l_0)]^{1/2}$ [see Eq. (33)] derived within the LG model does not capture the proper universal scaling behavior. Instead renormalization group schemes for the VBEG model have to be employed.

Nonetheless, our MFT results for the scaling function ϑ within the VBEG model and for $X=X_t$, if matched with respect to its amplitude with the experimental data at the tricritical point $y=0$ and after adjusting the scaling variable y by a factor y_{th} such that the experimental and theoretical positions of the maximum of the scaling function are the same (which is achieved for $y_{th} \approx 0.065$), yield an adjusted scaling function $\bar{\vartheta}(y)$ which reproduces rather well the experimental data (see Fig. 11), especially near the maximum where interfacial effects are expected to be dominant. This observation is consistent with our interpretation that the formation of this maximum is dominated by the occurrence of the soft mode phase which does not depend on the details of the surface fields. We note that according to Fig. 11 the experimental data nominally for $X=X_t$ more closely agree with the theoretical ones for $X=X_t-0.01$. This raises the question as to

whether the experimental ^{3}He concentration in the film is actually shifted relative to the bulk one.

B. Pure ^{4}He

The theoretical models discussed in the previous sections (VBEG and LG as lattice and continuum models, respectively) capture the *universal* features of the collective behavior close to critical (and tricritical) points, such as the Casimir force. (These models have no predictive power concerning nonuniversal properties.) The associated finite-size scaling functions acquire universal forms if expressed in terms of proper scaling variables, such as $L/\xi(\tau)$, where $\xi(\tau)$ is the correlation length which controls the large-distance exponential decay of the two-point correlation functions of the OP fluctuations *in the bulk* at the reduced temperature τ. In systems with discrete symmetry one has $\xi(\tau \to 0^-) = \xi_0^-(-\tau)^{-\nu}$ and $\xi(\tau \to 0^+) = \xi_0^+ \tau^{-\nu}$, where $\xi_0^\pm$ are *nonuniversal*, i.e., system-dependent, amplitudes such that the ratio ξ_0^+/ξ_0^- is *universal* (see, e.g., Ref. [41]). Accordingly, the scaling function maintains its universal character also as a function of $y=\tau(L/\xi_0^+)^{1/\nu}$ in the notation of Sec. IV or, alternatively, $\tau(L/\xi_0^-)^{1/\nu}$. However, in the case of pure ^{4}He, the bulk correlation length $\xi(\tau<0)$ below the λ transition is infinite due to Goldstone modes and therefore ξ_0^- cannot be defined directly from the behavior of $\xi(\tau<0)$. Alternatively, one might define a different length scale $\xi^T(\tau<0) = \xi_0^T(-\tau)^{-\nu}$ associated with the power-law decay of tranverse correlations in the superfluid phase, which is related to the superfluid density; the nonuniversal amplitude ξ_0^T forms a universal ratio with ξ_0^+ (see, e.g., Refs. [41,42]). For pure ^{4}He, experimental estimates of $(\xi_0^T)_{exp}$ range from 1.2 Å [43] to 3.6 Å [44], depending on the way it is measured. In view of this experimental uncertainty and of the complication related to the introduction of $\xi_0^T \propto \sqrt{u_0}\xi_0^+$ [42] within the MFT discussed in Sec. IV, we present the comparison between experimental data and the VBEG model in terms of the scaling variable y, which involves the nonuniversal amplitude ξ_0^+ the value of which is well assessed experimentally for ^{4}He, $(\xi_0^+)_{exp} = 1.43$ Å at saturated vapor pressure [45], and theoretically for the VBEG model, $\xi_0^+ = 0.41a$ within the present MFT, where a is the lattice spacing (see the end of Sec. IV A). Within the LG model one has an analytic expression for ξ_0^+ in terms of the parameters of the model [see Eq. (6.4) in Ref. [13] for ξ_0^+ obtained within the dimensional regularization scheme].

In Fig. 12 we compare the scaling function obtained from the experimental data for the case of pure ^{4}He [2] (for a film thickness $L=423$ Å [39]) with the MF scaling function $\vartheta_0(y)$ of the VBEG model which is universal for sufficiently thick films. The scaling functions are normalized by their absolute values $|\vartheta_{min}|$ at the minimum. In order to summarize all available theoretical results we report in the right inset of Fig. 12 the comparison between the experimental data for $T>T_\lambda$ and the scaling function obtained from the field-theoretical ϵ expansion ($\epsilon=4-d$) [13] as follows: The scaling function $\Theta_{+O,O}(y_+)$ of the finite-size contribution of the renormalized free energy f provided in Eq. (6.12) of Ref. [13] has been re-expressed for $N=2$ (XY model) as a function
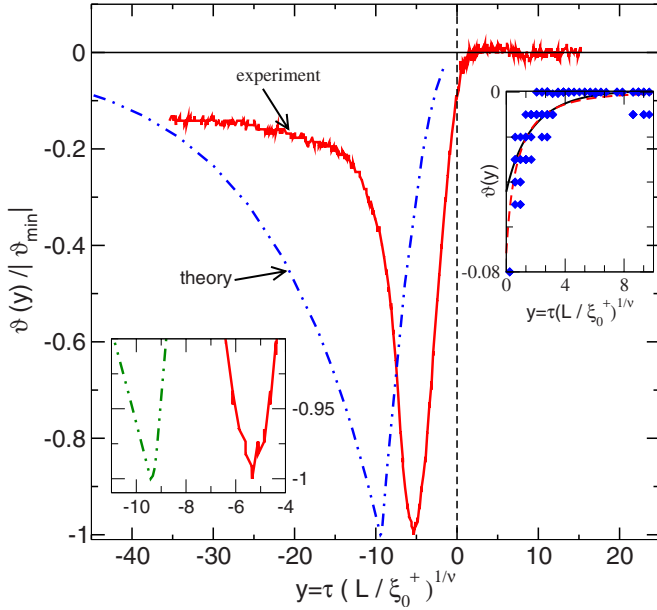
FIG. 12. (Color online) Normalized mean-field scaling function $\vartheta_0(y)$ for the limiting case of the VBEG model (on a lattice with $\bar{L}=60$) corresponding to pure ^{4}He compared with the experimental data $(\vartheta)_{exp}$ [2] in terms of the proper scaling variable $y = \tau(L/\xi_0^+)^{1/\nu}$ using $(\xi_0^+)_{exp}=1.43$ Å for pure ^{4}He [45] and $\nu=0.67$. These are the universal forms of the scaling function ϑ_0. The inset on the left shows a magnification of the main plot close to the minimum. According to the analysis presented in Sec. IV B (see also Fig. 9), the position $y_m(\bar{L})$ of the minimum of the theoretical curve in the scaling limit $\bar{L}=\infty$ approaches the value $-\pi^2$. In the inset on the right the experimental data (diamonds) above the critical temperature are compared with the scaling functions for the three-dimensional XY model in a slab obtained from the ϵ expansion (see the main text: the solid (dashed) line corresponds to the [1,0] ([0,1]) Padé approximant). Due to the experimental resolution $(\vartheta)_{exp}$ takes only discretized values.

of $y = \tau(L/\xi_0^+)^{1/\nu}$ via $y_+ = y^{1/2}(1+\epsilon/10 \ln y) + O(\epsilon^2)$ [where y_+ is defined after Eq. (4.6) in Ref. [13]]. The resulting expression $\Theta_{+O,O}(y) = \theta_0(y) + \epsilon\theta_1(y) + O(\epsilon^2)$ is then extrapolated to three dimensions $\epsilon=1$ either as $\Theta_{+O,O}^{[1,0]}(y) = \theta_0(y) + \epsilon\theta_1(y)$ (yielding the solid line in the inset) or $\Theta_{+O,O}^{[0,1]}(y) = \theta_0(y)/[1 - \epsilon\theta_1(y)/\theta_0(y)]$ (dashed line), corresponding to the Padé approximants [1,0] and [0,1]. The scaling function of the Casimir force is then provided by $\vartheta(y) = (d-1)\Theta_{+,O,O}(y) - (y/\nu)\Theta'_{+,O,O}(y)$ where $d=3$ and $\nu \simeq 0.67$ (see, e.g., Table 19 in Ref. [41]), accounting for the actual expression of the scaling variable y in three dimensions.

Discrepancies, such as the position y_m of the minimum, the shape of the scaling function for $y > y_m$, the behavior for $y \to -\infty$, and the nonvanishing of ϑ^{exp} for $y \geq 0$, can be attributed to fluctuation effects neglected in the present MF approach. Field-theoretic renormalization group calculations beyond MFT yield a quantitative agreement with the experimental data for $y \geq 0$ [10,13,14] (see Fig. 12); however, so far this field-theoretical approach cannot be extended to the case $y < 0$ [38]. From the analysis of Sec. IV B it follows that for fixed L the position $y_m = -\pi^2 \simeq -9.87$ of the minimum is

associated with the critical temperature $T_c(L)$ of the film. The experimental data exhibit the position of the minimum at $x_{min} = -9.8 \pm 0.8$ Å$^{1/\nu}$, where $x \equiv \tau L^{1/\nu}$ [2,7], corresponding to $(y_m)_{exp} \equiv x_{min}/(\xi_0^+)_{exp}^{1/\nu} \simeq -5.7 \pm 0.5$ which is consistent with the experimental indication in the sense that the onset of superfluidity in the films occurs within the range -12 Å$^{1/\nu} \lesssim x \lesssim -7$ Å$^{1/\nu}$ [7], i.e., $-8 \lesssim y \lesssim -5$. But these values of y are considerably larger than the value $-\pi^2$ predicted by the LG approximation. In spite of the shortcomings mentioned above the comparison between the experimental and theoretical scaling function is nonetheless encouraging. The present MF approach does not address the issue that $|\vartheta_{min}/\vartheta(0)|_{exp} \simeq 20$ [4,7] whereas theoretically this ratio is $\simeq 1$ for periodic BCs [38]; it is difficult to expect that this ratio reaches the experimental value 20 corresponding to the actual (O,O) BC.

In passing we mention that in Ref. [36] the comparison between Eq. (56) and the experimental data of Refs. [2,7] is seemingly affected by an inconsistent normalization of the experimental and theoretical scaling functions which are actually plotted as a function of $\tau(L/\xi_0^T)^{1/\nu}$ (with ξ_0^T taken from Ref. [43]) and $\tau(L/\xi_0^+)^{1/\nu}$, respectively. This artificially reduces the resulting discrepancy between the experimental and theoretical results in comparison to the one displayed in Fig. 12.

VI. SUMMARY AND OUTLOOK

Based on mean-field analyses of the vectorized Blume-Emery-Griffiths model and of the continuum Landau-Ginzburg theory as well as by applying renormalization-group analyses we have obtained the following main results:

(i) By using mean-field theory, near the tricritical point (Fig. 4) we have calculated the scaling functions of the Casimir force within the continuum Landau-Ginzburg theory [Eq. (1)] for the $O(2)$ model of ^{3}He-^{4}He films of thickness L (see Figs. 1 and 2). The scaling functions depend on two relevant scaling variables u_0 and r_0 [see Eq. (18)]. By fitting the amplitude of the scaling variable and the amplitude of the Casimir force, which remains undetermined within the LG mean-field approach, one finds a reasonable agreement with the experimental data along the thermodynamic path of constant tricritical concentration of ^{3}He (see Fig. 3).

(ii) The application of field-theoretic renormalization-group analysis in spatial dimension $d=3$ yields the correct asymptotic leading behavior of the Casimir force at the tricritical point. As a function of the film thickness L it has the form of a power law $\sim L^{-3}$ multiplied by the square root of the logarithm of L and by the universal Casimir amplitude [Eq. (23)].

(iii) Using the field-theoretic renormalization-group analysis we have derived the form of the finite-size scaling for the Casimir force in the vicinity of the tricritical point and have obtained renormalized mean-field scaling functions (see Figs. 1 and 2). It turns out that also one of the scaling variables acquires a logarithmic correction [Eq. (33)].

(iv) Using mean-field approximation we have calculated the scaling function of the Casimir force within the vectorized Blume-Emery-Griffith lattice model of ^{3}He-^{4}He mix-

tures along the thermodynamic paths of fixed ^{3}He concentrations (see Figs. 4–6). For concentrations of ^{3}He close to the tricritical concentration our results are in a qualitative agreement with the available experimental data (see Figs. 3, 5, and 11). Our calculations also predict the crossover behavior of the Casimir force along the line of critical points connecting the tricritical point and the λ transition for pure ^{4}He. We have found that the pronounced maximum of the Casimir force, which occurs below the tricritical temperature, is associated with the formation of a soft mode phase within the film (see Figs. 7 and 8).

(v) We have analyzed the limiting case of the VBEG model which corresponds to the classical *XY* model for pure ^{4}He. Within mean-field theory we have been able to show that for sufficiently thick films the scaling functions as obtained from the lattice model for the Casimir force are in an agreement with the ones obtained from the continuum $O(2)$ Landau-Ginzburg theory (see Fig. 9). The encouraging comparison of the former with the experimental data is displayed in Fig. 12.

As an outlook we propose to test experimentally the scaling of the Casimir force for different thicknesses of the wetting films by taking into account logarithmic corrections. Moreover, it appears to be promising to study experimentally in more detail the crossover of the Casimir forces between their tricritical behavior and their critical behavior near the λ transition and to compare it with the theoretical predictions presented here.

ACKNOWLEDGMENTS

[1] H. B. Casimir, Proc. K. Ned. Akad. Wet. **51**, 793 (1948).

[2] R. Garcia and M. H. W. Chan, Phys. Rev. Lett. **83**, 1187 (1999).

[3] A. Mukhopadhyay and B. M. Law, Phys. Rev. Lett. **83**, 772 (1999).

[4] R. Garcia and M. H. W. Chan, Phys. Rev. Lett. **88**, 086101 (2002).

[5] T. Ueno, S. Balibar, T. Mizusaki, F. Caupin, and E. Rolley, Phys. Rev. Lett. **90**, 116102 (2003); R. Ishiguro and S. Balibar, J. Low Temp. Phys. **140**, 29 (2005).

[6] M. Fukuto, Y. F. Yano, and P. S. Pershan, Phys. Rev. Lett. **94**, 135702 (2005).

[7] A. Ganshin, S. Scheidemantel, R. Garcia, and M. H. W. Chan, Phys. Rev. Lett. **97**, 075301 (2006).

[8] M. E. Fisher and P. G. de Gennes, C. R. Seances Acad. Sci., Ser. B **287**, 207 (1978).

[9] M. Krech, *The Casimir Effect in Critical System* (World Scientific, Singapore, 1994); J. Phys.: Condens. Matter **11**, R391 (1999); M. P. Nightingale and J. O. Indekeu, Phys. Rev. Lett. **54**, 1824 (1985); J. Indekeu, J. Chem. Soc., Faraday Trans. 2 **82**, 1838 (1986).

[10] M. Krech and S. Dietrich, Phys. Rev. Lett. **66**, 345 (1991); **67**, 1055 (1991).

[11] V. Privman, in *Finite Size Scaling and Numerical Simulation of Statistical Systems*, edited by V. Privman (World Scientific, Singapore, 1990), p. 1; J. G. Brankov, D. M. Danchev, and N. S. Tonchev, *The Theory of Critical Phenomena in Finite-Size Systems—Scaling and Quantum Effects* (World Scientific, Singapore, 2000).

[12] H. W. Diehl, in *Phase Transitions and Critical Phenomena*, edited by C. Domb and J. L. Lebowitz (Academic, London, 1986), Vol. 10, p. 76.

[13] M. Krech and S. Dietrich, Phys. Rev. A **46**, 1886 (1992);

[14] M. Krech and S. Dietrich, Phys. Rev. A **46**, 1922 (1992).

[15] R. Zandi, J. Rudnick, and M. Kardar, Phys. Rev. Lett. **93**, 155302 (2004).

[16] E. K. Riedel, Phys. Rev. Lett. **28**, 675 (1972); E. K. Riedel and F. J. Wegner, *ibid.* **29**, 349 (1972).

[17] D. Lawrie and S. Sarbach, in *Phase Transitions and Critical Phenomena*, edited by C. Domb and J. L. Lebowitz (Academic, London, 1984), Vol. 9, p. 2.

[18] J.-P. Romagnan, J.-P. Laheurte, J.-C. Noiray, and W. F. Saam, J. Low Temp. Phys. **30**, 425 (1978).

[19] A. Maciołek and S. Dietrich, Europhys. Lett. **74**, 22 (2006).

[20] A. Maciołek, M. Krech, and S. Dietrich, Phys. Rev. E **69**, 036117 (2004), and references therein.

[21] E. Eisenriegler and H. W. Diehl, Phys. Rev. B **37**, 5257 (1988), and references therein.

[22] E. K. Riedel, Phys. Rev. Lett. **28**, 675 (1972).

[23] P. Leiderer, D. R. Watts, and W. W. Webb, Phys. Rev. Lett. **33**, 483 (1974).

[24] U. Ritschel and M. Gerwinski, Physica A **243**, 362 (1997).

[25] For critical systems in the film geometry the renormalization of the free energy was discussed in Ref. [13]. It was shown that additive terms give rise to finite-size contributions to the free energy which are analytic in $t=(T-T_c)/T_c$ and exponentially small as a function of L.

[26] D. J. Amit, *Field Theory, the Renormalization Group and Critical Phenomena* (McGraw-Hill, New York, 1978).

[27] G. M. Bell and D. A. Lavis, *Statistical Mechanics of Lattice Models* (Ellis Horwood Ltd., Chichester, 1989).

[28] P. M. Chaikin and T. C. Lubensky, *Principles of Condensed Matter Physics* (Cambridge University Press, Cambridge, UK, 1995).

[29] A. Crisanti and L. Peliti, J. Phys. A **18**, L543 (1985).

[30] A. O. Parry and R. Evans, Phys. Rev. Lett. **64**, 439 (1990).

[31] R. Evans and J. Stecki, Phys. Rev. B **49**, 8842 (1994); A. O. Parry and R. Evans, Phys. Rev. Lett. **64**, 439 (1990).

[32] M. E. Fisher, J. Chem. Soc., Faraday Trans. 2 **82**, 1569 (1986).

[33] J. M. Kosterlitz and D. J. Thouless, J. Phys. C **6**, 1181 (1973).

[34] A. Gambassi and S. Dietrich, J. Stat. Phys. **123**, 929 (2006).

[35] M. E. Fisher and H. Nakanishi, J. Chem. Phys. **75**, 5857 (1981).

[36] R. Zandi, A. Shackell, J. Rudnick, M. Kardar, and L. P. Chayes, e-print arXiv:cond-mat/0703262.

[37] D. Dantchev and M. Krech, Phys. Rev. E **69**, 046119 (2004).

[38] D. Dantchev, M. Krech, and S. Dietrich, Phys. Rev. Lett. **95**, 259701 (2005).

[39] R. Garcia (private communication).

[40] H. A. Kierstead, J. Low Temp. Phys. **24**, 497 (1976).

[41] A. Pelissetto and E. Vicari, Phys. Rep. **368**, 549 (2002).

[42] P. C. Hohenberg, A. Aharony, B. I. Halperin, and E. D. Siggia, Phys. Rev. B **13**, 2986 (1976).

[43] G. G. Ihas and F. Pobell, Phys. Rev. A **9**, 1278 (1974).

[44] A. Singsaas and G. Ahlers, Phys. Rev. B **30**, 5103 (1984).

[45] W. Y. Tam and G. Ahlers, Phys. Rev. B **32**, 5932 (1985), Table XI.